

Universität Tübingen

**Bachelor
Geowissenschaften
Umweltnaturwissenschaften**

**Modul
GEOPHYSICS 1&2**

**Course Notes
*for use in this lecture only***

(figures are partly taken from books and journals but not explicitly cited for simplicity)

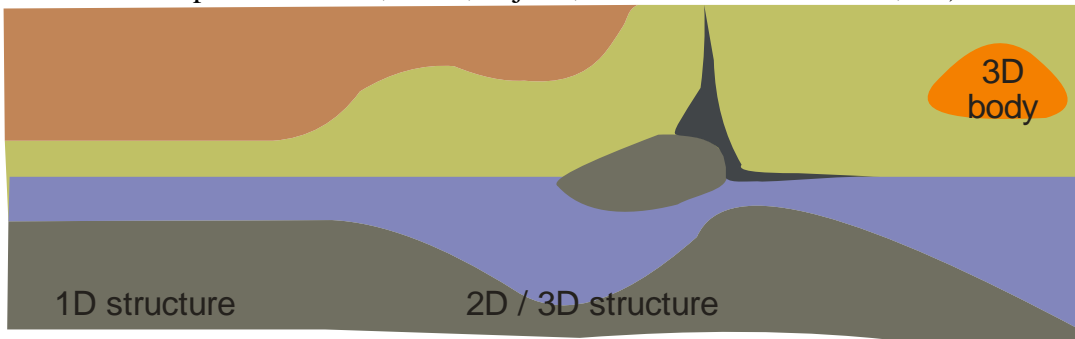
**Erwin Appel
2013/2014**

A Introduction

A.1 Aims of geophysical investigation

- Analysis of subsurface structures

(layers or more complex structures, voids, objects, zones of contamination, etc)



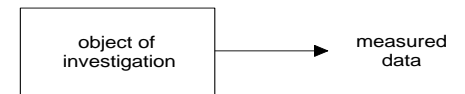
A 1D (*one-dimensional*) structure shows horizontal layer boundaries (any other cross-section shows the same structure). A 2D structure is given when layers are dipping or undulating but showing the same structure in all parallel cross-sections (perpendicular to the strike direction of the structure). In a 3D structure the depth and/or shape of dipping layer boundaries are different in parallel cross-sections). More isometric structures are also 3D structures but usually termed 'bodies' (*Störkörper*). Note: Of course there is no unlimited area with a 1D or 2D structure – the criteria is that such a structure exists to a distance that influences the measured data.

- Determination of physical (can be directly measured) or geological (have to be derived from geophysical data by suitable transfer functions) parameters
(seismic velocities, electrical conductivity, density, porosity, hydraulic conductivity, water/oil content, clay/sand content, weathering degree, etc.)
- Monitoring (repeated measurements) of subsurface processes
(spread of tracer or contaminants, compaction of soils, parameter changes during remediation of contaminated sites, etc.)

A.2 Basic concepts of geophysical measurements, inversion & interpretation

A.2.1 Passive and active measurements

Passive measurements use naturally existing physical fields (e.g., gravity field, magnetic fields, natural radiation) or natural effects (e.g. earthquakes)



General concept of passive measurements

In active measurements one has to apply a source (e.g., explosion to create seismic waves, electric current injected or induced into the ground).



General concept of active measurements

A.2.2 Arrangement of measurements

- Sounding
 - measurements are carried out at one location → function of depth $f(z)$
- Profiling
 - measurements are carried out along a profile
 - one data per location is measured → function of position along profile $f(x)$
 - several data per location are measured → function of position along profile and of depth $f(x,z)$
- Mapping
 - measurements are carried out in an area
 - one data per location is measured → function of position in the measurement area $f(x,y)$
 - several data per location are measured → function of position in the measurement area and of depth $f(x,y,z)$
- Borehole measurements
 - measurements in single borehole (logging) → function of depth $f(z)$
 - crosshole measurements → function of depth and of direction between boreholes $f(x,z)$

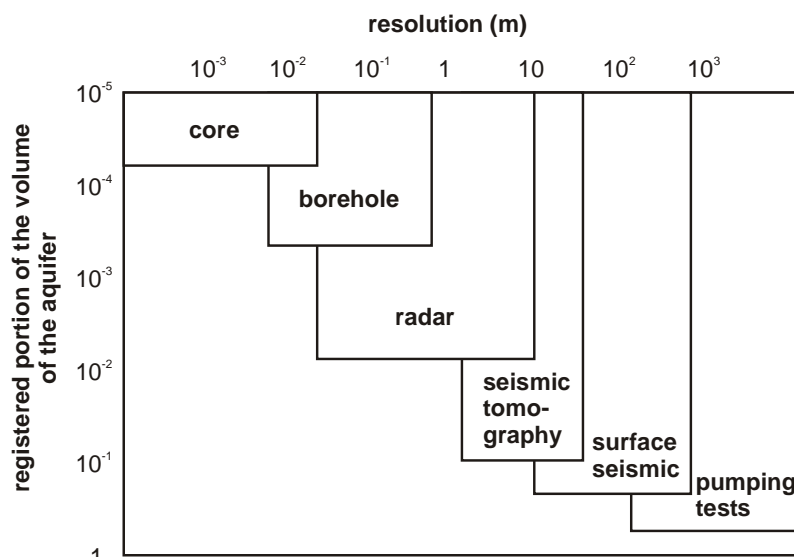
Note: here we generally use x and y as horizontal coordinates and z as the depth coordinate

A.2.3 Investigation methods and relevant parameters

Method	Physical parameter controlling results
Gravimetry methods	Density
Geomagnetic methods	Magnetic susceptibility, magnetic remanence
geoelectrical (resistivity) methods	electrical resistivity
electromagnetic methods	conductivity or resistivity, permittivity
seismic methods	wave velocities, absorption coefficient, reflection coefficient
geothermal methods	thermal conductivity
radiometric methods	natural radiation, absorption of gamma or neutron rays

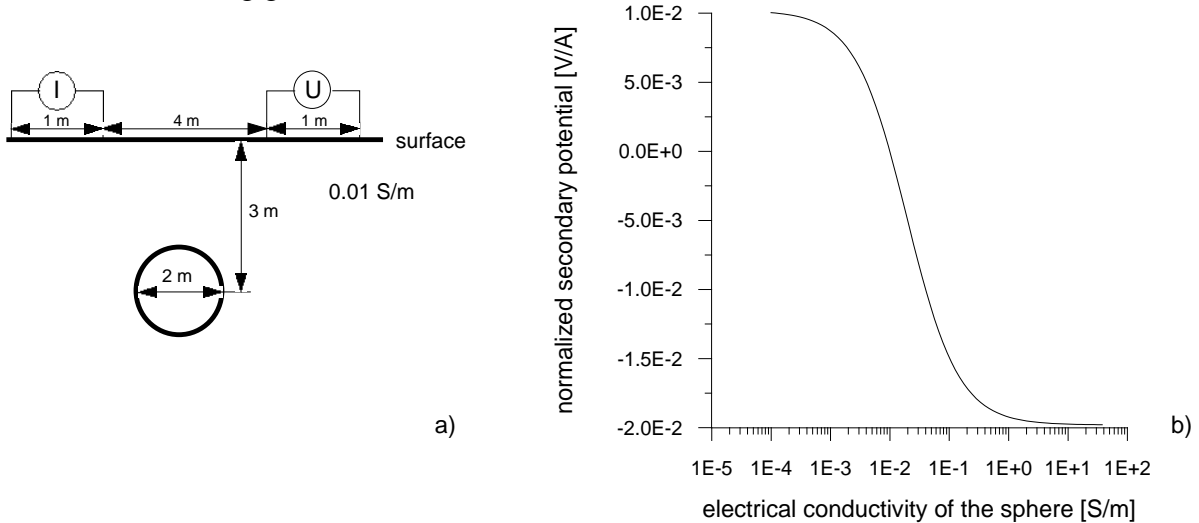
A.2.4 Investigation range, resolution and sensitivity

Different methods have different potential for the spatial range investigated and the resolution obtained. If the dimension of investigation (spatial range affecting the measurement) is large, then usually the resolution is low. When investigating a small dimension with high resolution there is the problem whether or how the result is valid for a larger area (*up-scaling*); up-scaling is mostly a very difficult task.



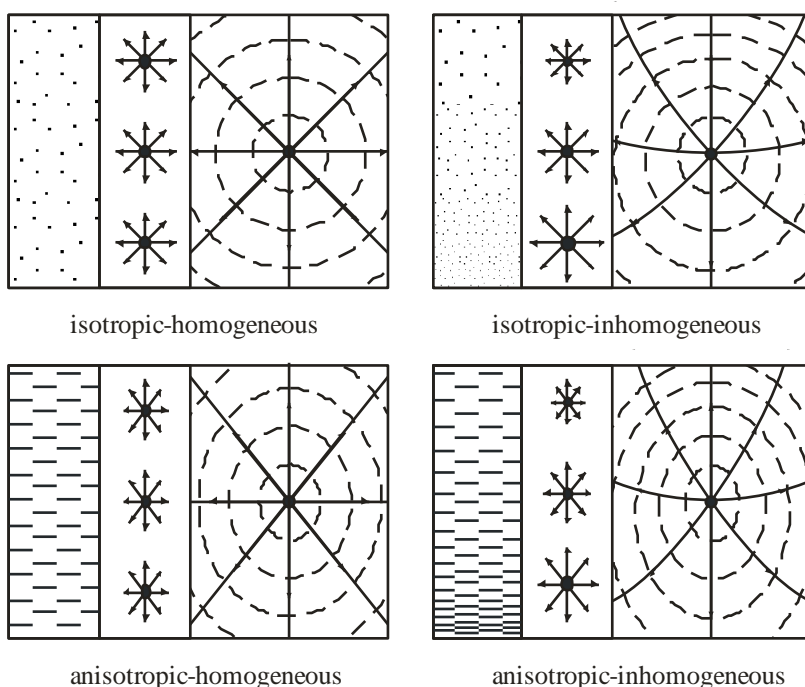
Schematic principle of resolution and dimension of investigation

The sensitivity of measurements on parameter distribution is a critical factor for evaluating the possibility of applying a method and interpreting results. For the example below of an electrical measurement (*here the difference of electrical conductivity σ of a buried sphere and the surrounding material is the important parameter influencing the measured data*) the method gives a more significant result about the buried sphere when the sphere has a higher σ than the surrounding ground material.

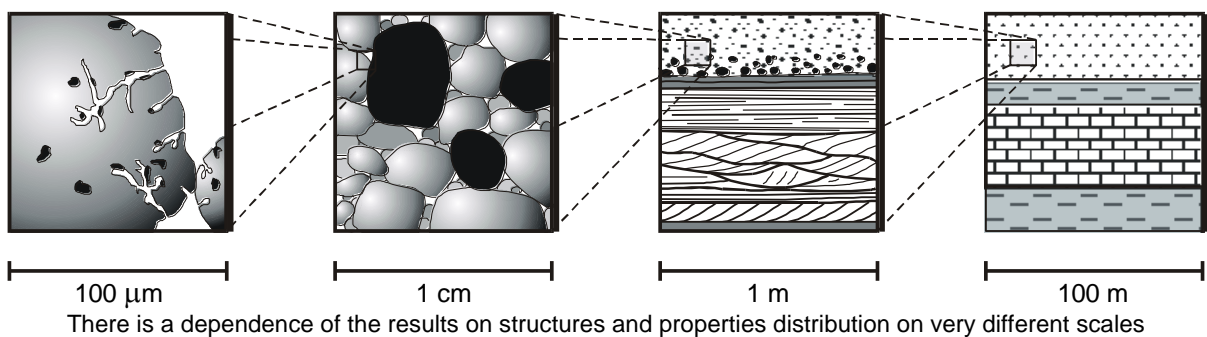


Influence of a sphere buried in 3m depth in a ground with conductivity of 0.01 S/m. Results of the deviation of the potential (U) difference (voltage) normalized to the value measured for a homogeneous ground are shown for different conductivities in the range of about 0.0001 to 100 S/m (a 4-point dipole-dipole electrode array is used in the example; see chapter D).

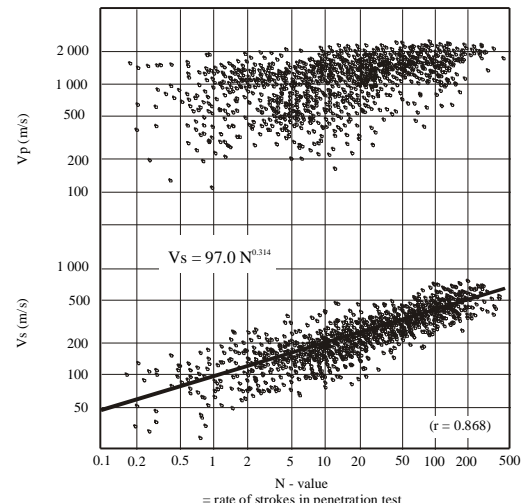
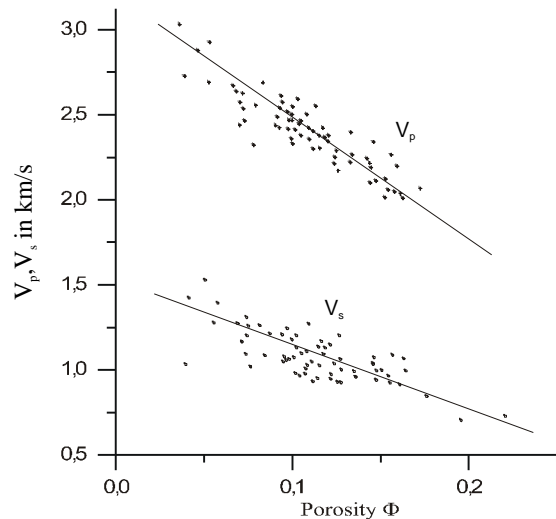
Measured results may provide data or parameter distributions which are homogeneous or inhomogeneous (spatial differences) or isotropic or anisotropic (directional differences). The examples given below may be representative for pore space distribution (left), seismic wave velocities (middle) and field of an electrical charge (right).



Whether a parameter distribution is inhomogenous or anisotropic also depends on the dimension of the area that is considered.



Transformation of geophysical parameters into geological, hydraulic or geotechnical parameters can be attempted by models (analytical or numerical) or by empirical relationships (see example below).



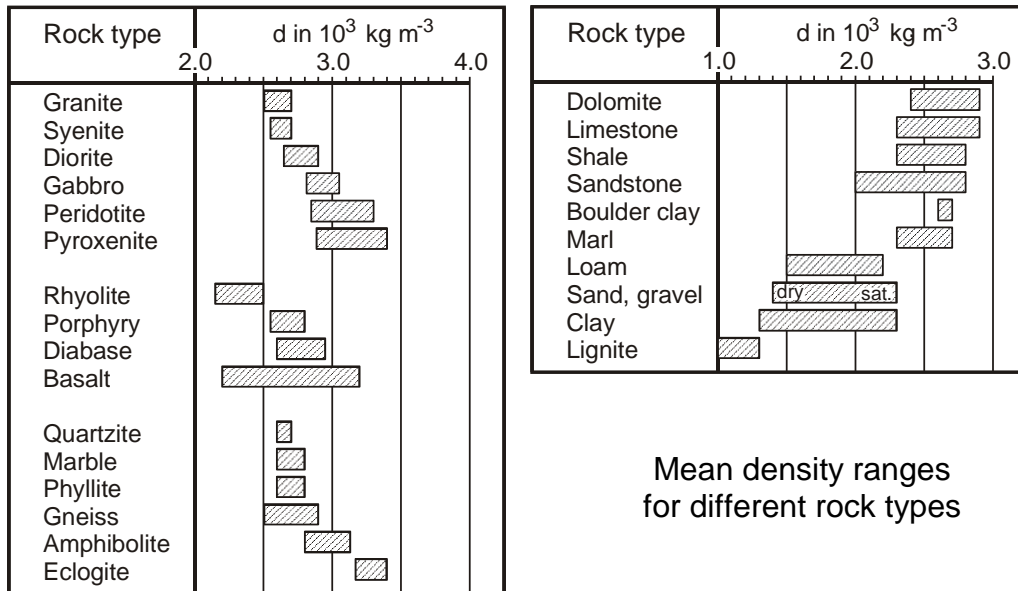
Empirical relations between measured geophysical parameters and other properties can be more or less between different parameters. The given examples are seismic wave velocities versus porosity (left) and N value (higher N values denote harder material) in the cone penetration test (right).

B Gravimetry

B.1 Fundamentals

The relevant (geo)physical parameter causing difference in gravity is **density**.

Mostly ρ [kg/m³] is used as a symbol for density; however, to avoid confusion with resistivity in chapter D we use here “**d**” for density.



Gravitational force F between the two point masses M and m

[valid also for homogeneous spheres and **spherical shells**; approximately valid for $r \gg$ dimension of masses]

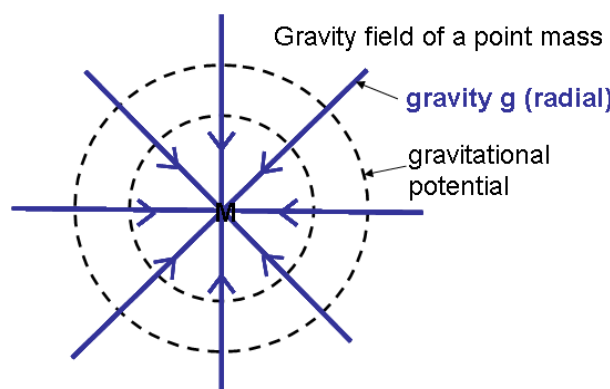
$$F = f \frac{m \cdot M}{r^2}$$

(gravitation constant $f = 6,672 \cdot 10^{-11} \text{ m}^3 \text{kg}^{-1} \text{s}^{-2}$; distance r between the masses M and m)

Gravitational acceleration \mathbf{g} (short: *gravity*): $\mathbf{g} = f \frac{\mathbf{M}}{r^2} = -\mathbf{grad}U$; $[\mathbf{g}] = \text{mgal} = 10^{-5} \text{ m/s}^2$

for point mass (radial field geometry of \mathbf{g}): $\mathbf{g} = -\frac{dU}{r}$ U: Gravitational potential

Gravitational potential for a point mass: $U = f \frac{M}{r}$

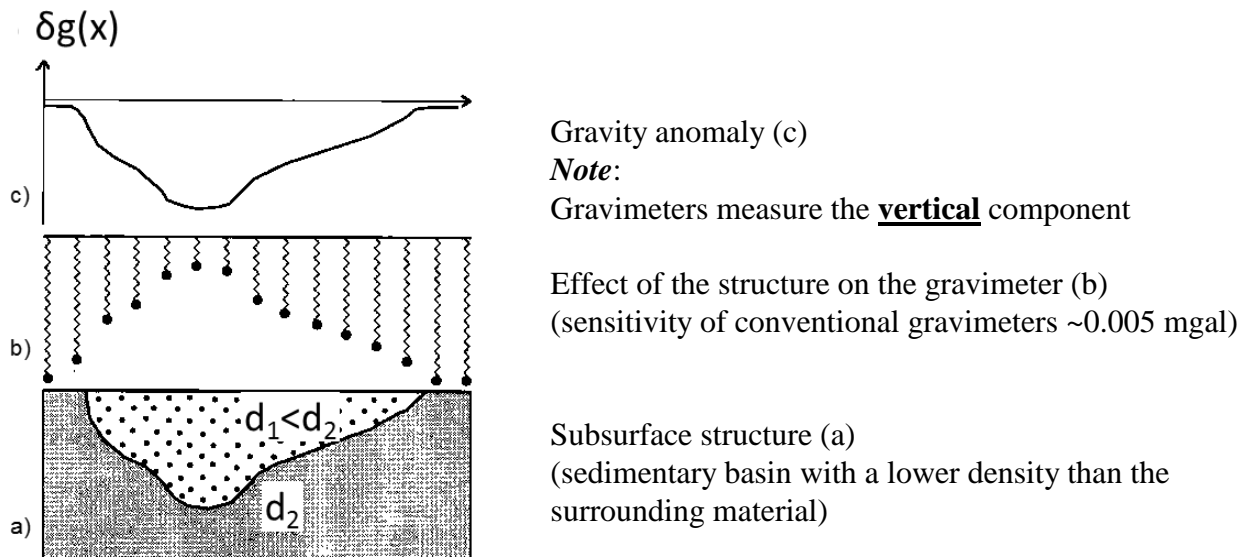


Note:
F and g are vectors,
while U is a scalar

B.2 Gravimetric measurements and interpretation

B.2.1 Principle of gravity measurements

A variation in density in the subsurface (being either a 1D, 2D, 3D structure or a more isometric body) creates an anomaly in the gravity on a profile at surface crossing that area.



B.2.2 Simple interpretation: locating an object, determination of maximum depth

Locating an object (e.g. a cavity) can be reasonably done by the position of the maximum anomaly value.

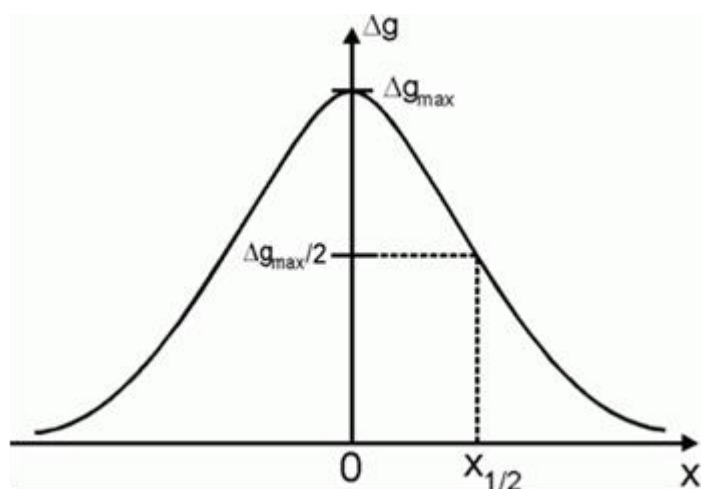
For depth estimation one can use the half-width of the measured anomaly.

The half-width HW ($=2 \cdot X_{1/2}$ in the figure) can be used to estimate the **maximum depth** t :

$$t \approx 2/3 \text{ HW} \text{ (for sphere);}$$

$$t \approx 1/2 \text{ HW} \text{ (for 2D cylinder)}$$

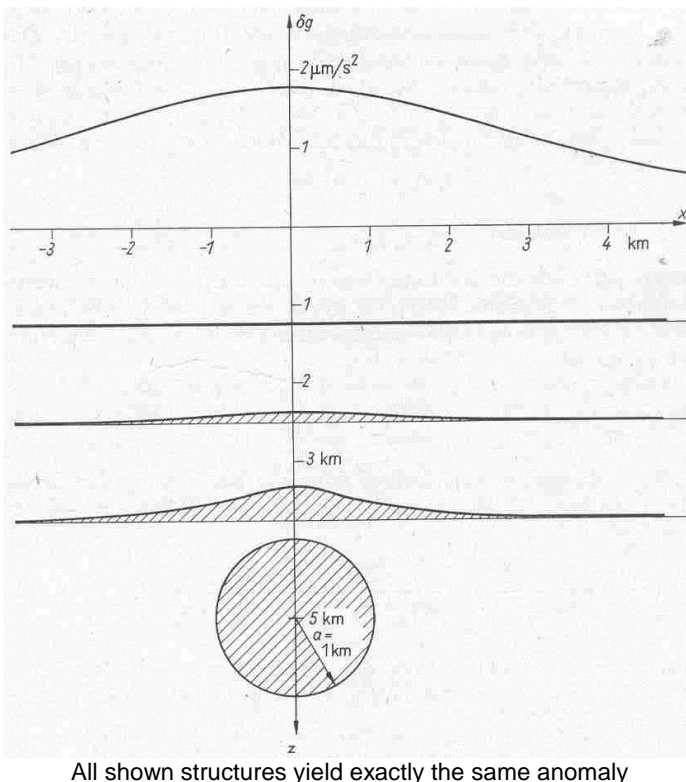
Shape of the body unknown
 → maximum possible depth $\sim 2/3$ HW



Model your sphere at:

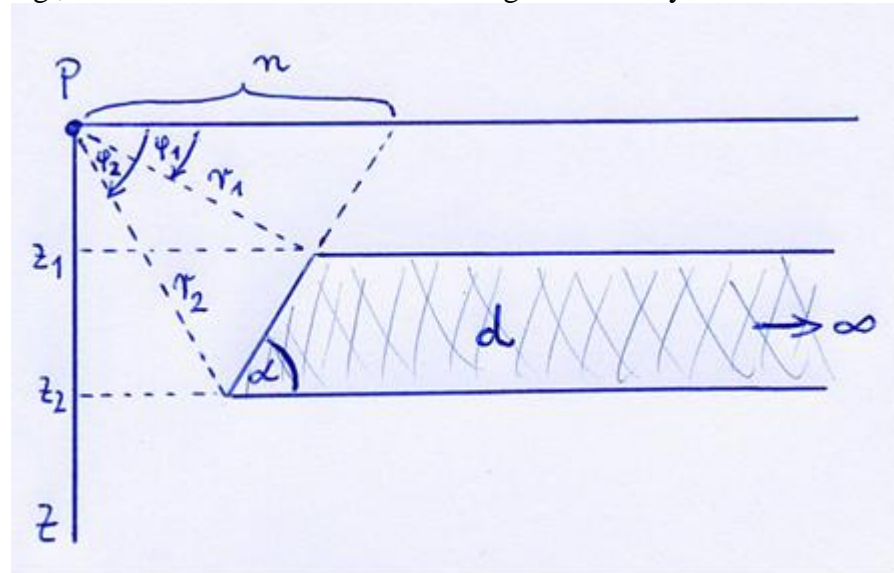
http://www.tankonyvtar.hu/hu/tartalom/tamop425/0033_SCORM_MFGFT6001T-EN/sco_01_11.scorm

B.2.3 Problem of equivalence



B.2.4 Forward modelling of structures

e.g., Calculation of 2D-anomalies using the anomaly of a half-infinite plate:



$$g_z(P) = 2 f d \{ -n \sin \alpha [(\varphi_2 - \varphi_1) \cos \alpha + \ln(r_2/r_1) \sin \alpha] + [z_2 \varphi_2 - z_1 \varphi_1] \}$$

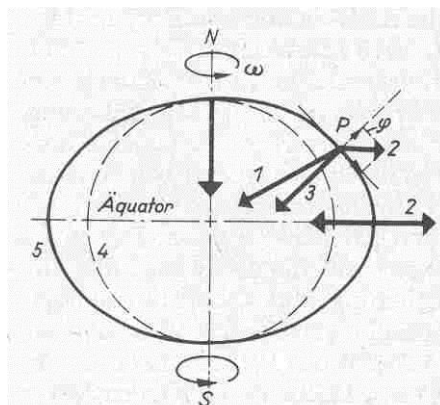
All 2D structures can be calculated by adding / subtracting half-infinite plates
(by defining corner points of a body)

For a simple modelling program see <http://www.gravity.uni-kiel.de/Software/Mod2D.htm>

Question: How to calculate 3D-anomalies?

B.3 Reduction of measured gravity data

Rotating Earth:
the reference ellipsoid
=Earth's normal
gravity potential field



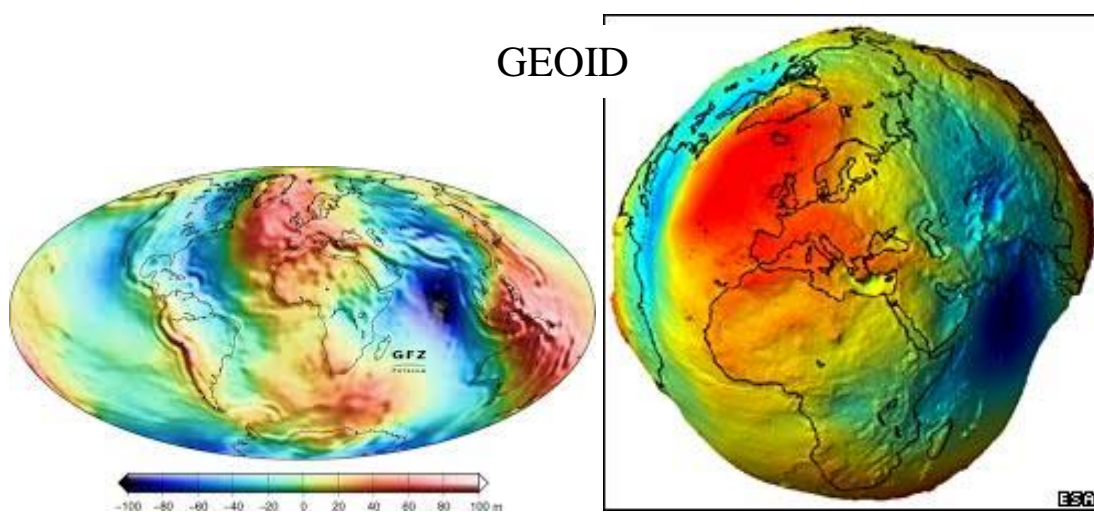
- 1 – acceleration from Earth's mass
- 2 – centrifugal acceleration
- 3 – resulting gravity g as a function of latitude
- 4 – surface of a sphere
- 5 - surface of real Earth (approached by an ellipsoid)

Vertical gradient (fre-air gradient) of the normal field (at Earth's surface): **0.3086 mgal/m**
To use the sensitivity of a gravity meter (0.01 mgal for land surveys) one must determine the elevation of the measurement point to an accuracy of 3 cm.

North-south gradient of the normal field (at Earth's surface): ~0.8 mgal/km (at 45° latitude)
The gradient varies with latitude (highest at 45°).

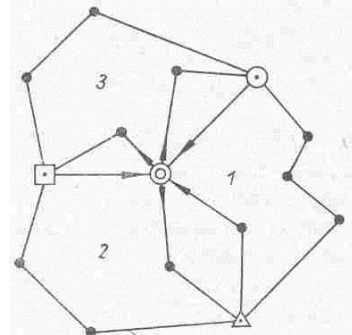
Difference of normal field between pole ($g \sim 9.83 \text{ m/s}^2$) and equator ($g \sim 9.78 \text{ m/s}^2$) is ~5.18 gal

The equipotential field can be approached by an ellipsoid best fitting to the shape of the Earth (**reference ellipsoid**). The true equipotential field, however, is much more complex, and is termed the **GEOID**. Deviations of the Geoid from the reference ellipsoid are termed geoid undulations (they are in the order up to 100 m).



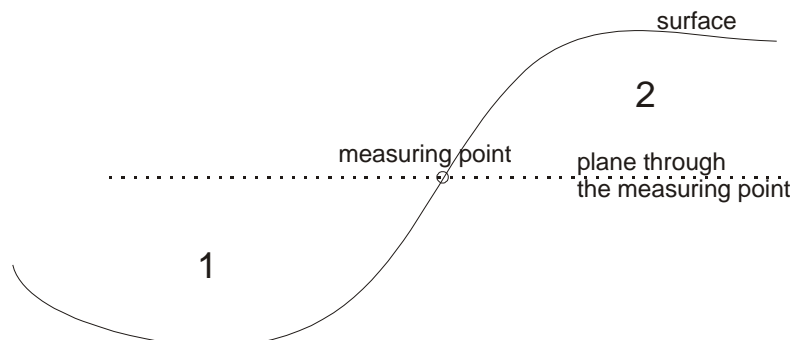
Geoid undulation map (left) and strongly enhanced 3D visualization of the Geoid

Time variations arise from Earth tides (effects up to 0.29 mgal) and the drift of the instrument.



Principle of repeated measurements at a **reference point** (base station) in order to correct for tidal effects and instrument drift. The determined variation with time is used to correct all the measuring data by time interpolation (so recording time is required for all measured points).

Principle of elimination of **topographic effects** (1–valleys are “filled”, 2–hills are “removed”) Both hills and valleys decrease the measured gravity value. For topographic reduction one has to remove the gravity effect of the hill’s mass and “fill” the valley.

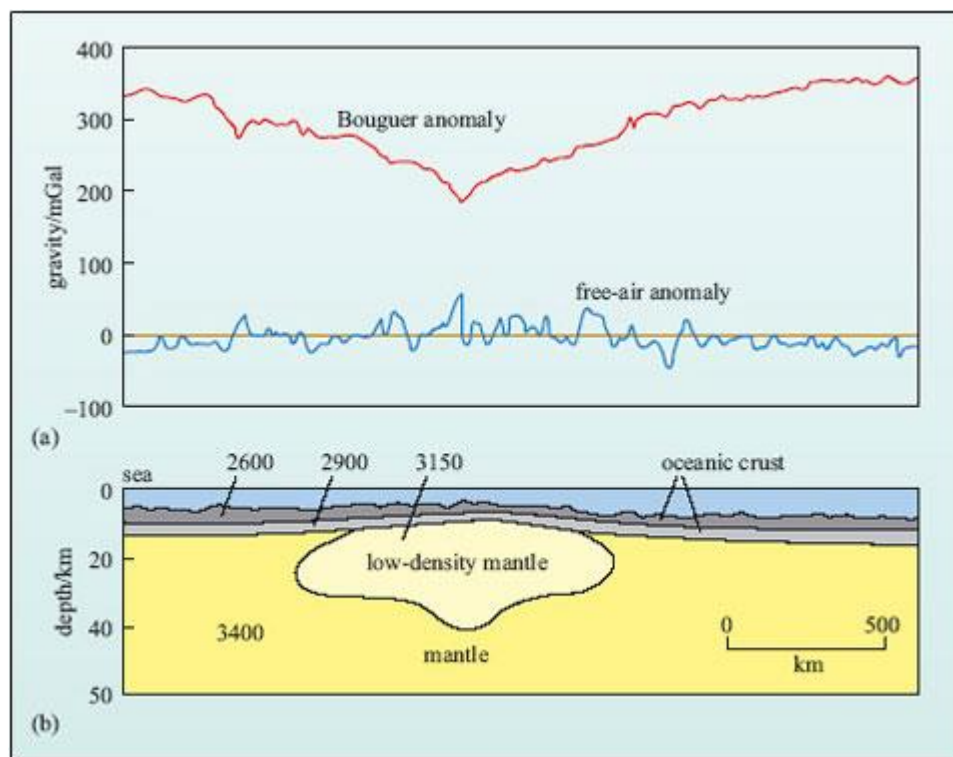


For measuring points at different levels (elevations) there remains the effect of the plate (**Bouguer Plate**) between the measurement level and a common reference level.

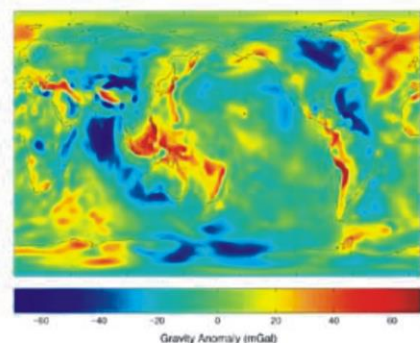
B.4 Examples

The anomaly resulting after reduction of the Earth’s normal gravity field (N-S and vertical gradients), time variations and topography effects is termed **Free Air Anomaly**.

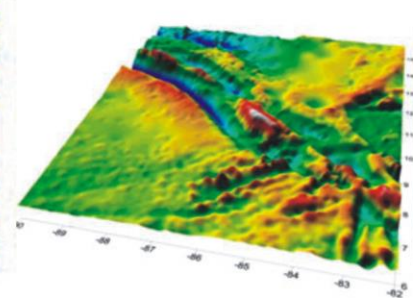
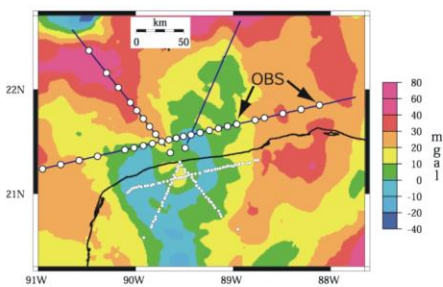
Removing additionally the effect of the plate (Bouguer plate) between the measurement point level and a fixed reference level is resulting in the **Bouguer Anomaly** (effect of Bouguer plate eliminated) or the **Isostatic Anomaly** (mass of Bouguer plate homogeneously distributed into the subsurface down to the depth of isostatic equilibrium).



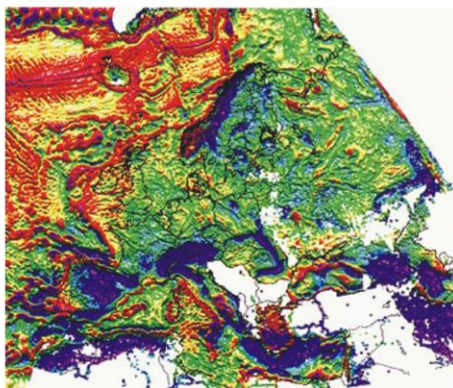
Free air anomaly (at sea level) and Bouguer anomaly (reference level in the crust) across a mid-oceanic ridge (the Bouguer anomaly at sea level would be identical with the free air anomaly; the free air anomaly along the sea bottom would show a clear positive anomaly like across mountain belts)



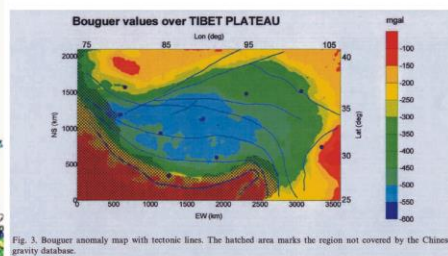
Erde - Freiluftanomalie

Anden - Land: Bouguer-Anomalie
Ozean: Freiluftanomalie

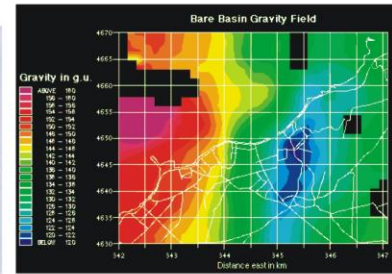
Chicxulub - Bouguer-Aanomalie



Europa - Bouguer-Anomalie



Tibet - Bouguer-Anomalie

Sedimentbecken
Bouguer-Anomalie

Examples for gravity anomalies from literature at different scales

C Magnetics

C.1 Fundamentals

C.1.1 Parameters

Magnetic field $B = \mu_0 \cdot H$; B [$T = Vs/m^2$] (T -Tesla), H [$A m^{-1}$]

$\mu_0 = 4\pi \cdot 10^{-7} Vs/Am$ magnetic permeability of free space

In geomagnetism mostly the B -field is used and given in $nT = 10^{-9} T$

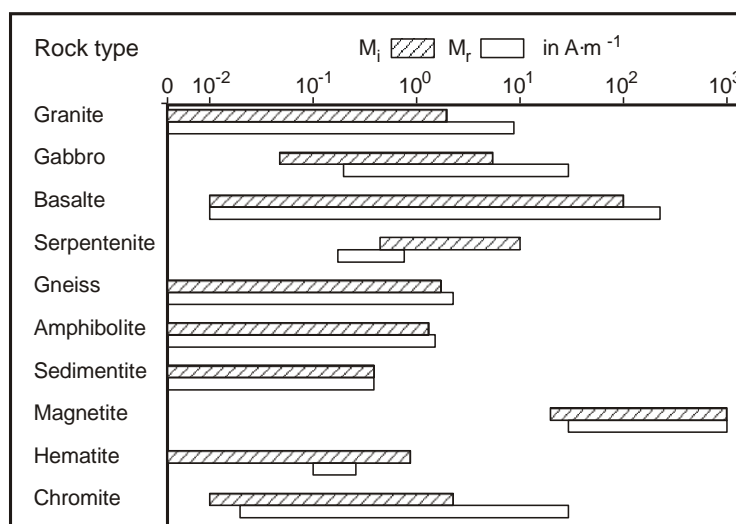
Magnetisation [$A m^{-1}$]; induced (M_i) and remanent (M_r) magnetisation

Magnetisation M is the vector sum of M_i and M_r

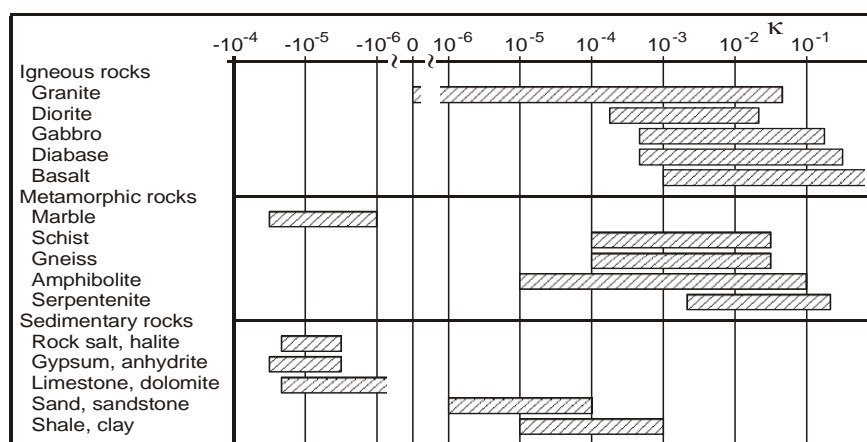
Magnetic moment m [$A m^2$] = $M \cdot V$ (V : volume)

Magnetic susceptibility κ [-] = M_i/H ;

B and H , M , m are *vectors*



Induced (M_i) and remanent (M_r) magnetization for some rock types; M of rocks varies over many orders



Mean range of susceptibility (κ) values for different rock types; also κ of rocks varies over many orders

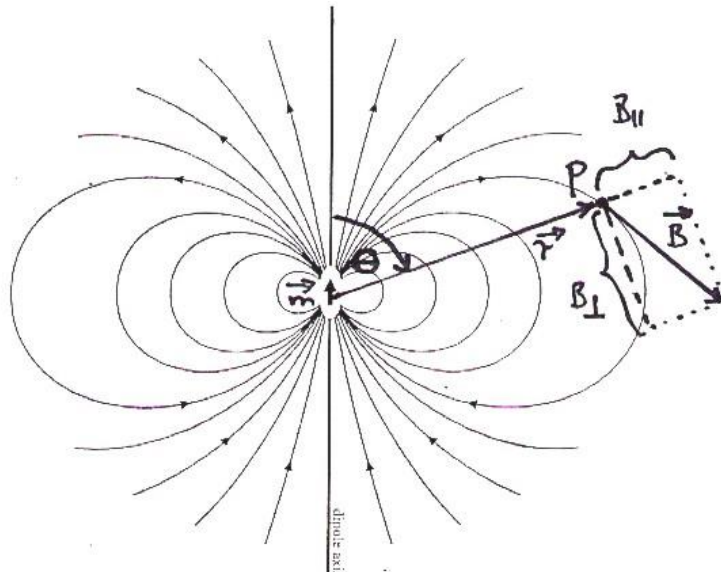
Remanent magnetization can be acquired by different processes. Its direction is usually not known.

Induced magnetization is caused by the Earth magnetic field B_{Earth} with M_i parallel to B_{Earth}

B_{Earth} is a global field and is known at the location of the measurement; thus the direction of M_i is also known.

C.1.2 Magnetic dipole

$\operatorname{div} \vec{B} = 0$ or $\oint \vec{B} \cdot d\vec{F} = 0$ means that magnetic B-field lines are always closed
(or in other words: there are no magnetic monopoles)



Magnetic dipole field

$$\Phi(P) = \frac{1}{4\pi} \cdot \frac{\vec{m} \cdot \vec{r}}{r^3} = \frac{1}{4\pi} \cdot \frac{m \cdot \cos \Theta}{r^2}$$

dipole potential

$$\vec{B} = -\mu_0 \cdot \operatorname{grad} \Phi$$

in polar coordinates:

$$B_z = -\mu_0 \cdot \frac{\partial}{\partial r} \Phi = \frac{\mu_0}{4\pi} \cdot \frac{2m \cdot \cos \Theta}{r^3}$$

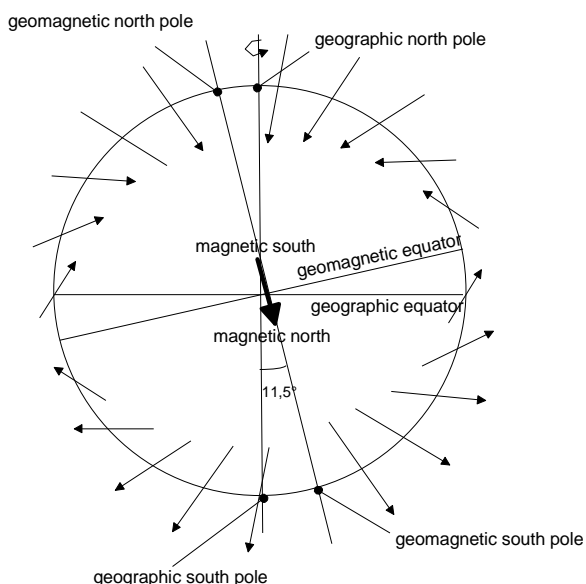
$$B_\perp = -\mu_0 \cdot \frac{1}{r} \cdot \frac{\partial}{\partial \Theta} \Phi = \frac{\mu_0}{4\pi} \cdot \frac{m \cdot \sin \Theta}{r^3}$$

$$B^2 = B_{\parallel}^2 + B_{\perp}^2$$

In a Cartesian coordinate system x-y the potential and components are calculated by:

$$\Phi(P) = \frac{1}{4\pi} \cdot \frac{\vec{m} \cdot \vec{r}}{r^3} = \frac{1}{4\pi} \cdot \frac{m_x \cdot x + m_y \cdot y}{(x^2 + y^2)^{3/2}}; \quad B_x = -\mu_0 \cdot \frac{\partial}{\partial x} \Phi \text{ and } B_y = -\mu_0 \cdot \frac{\partial}{\partial y} \Phi$$

C.1.3 Earth magnetic field



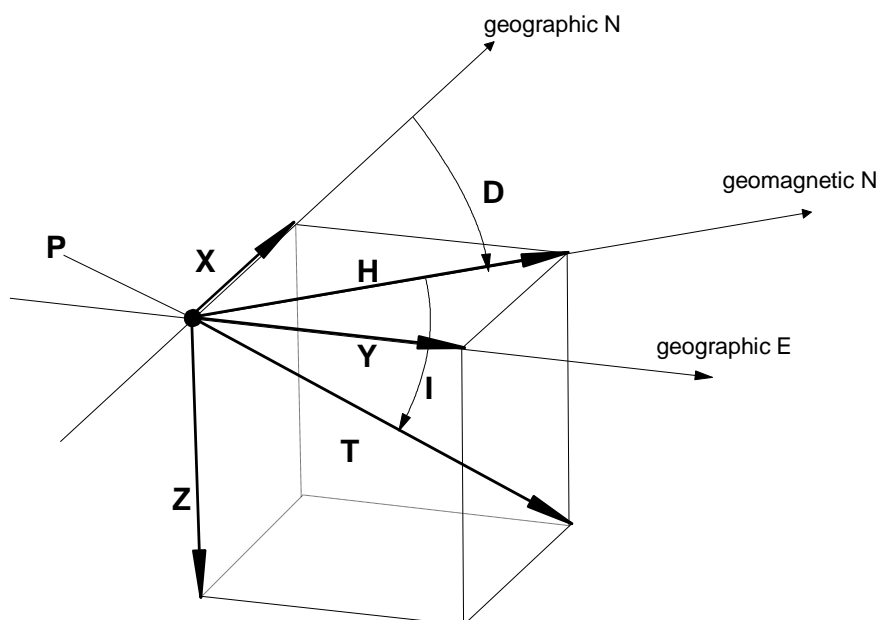
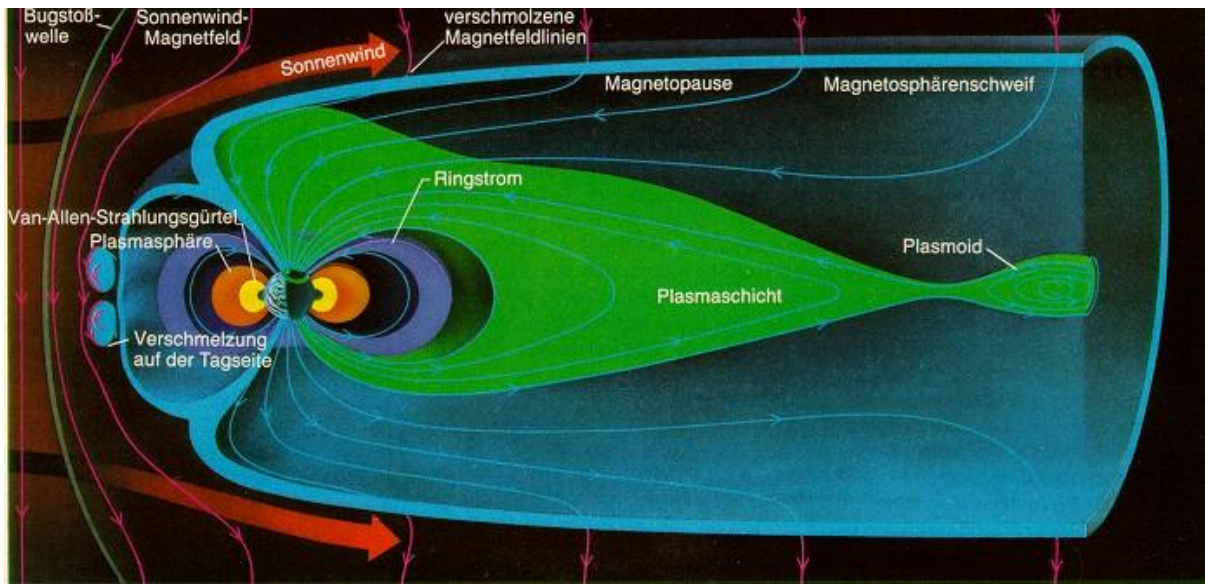
Present Earth magnetic field (dipole inclined in respect to the Earth's rotation axis) showing the field directions at the Earth's surface

B_{Earth} is about 60,000 nT at the magnetic poles.

The by far major contribution comes from a "dynamo" in the Earth's core creating a dipole like field.

There is also a contribution of an external field caused by the solar wind. It varies about 30 nT during normal days but can vary up to more than 1000 nT during “magnetic storms”.

The Earth's inner magnetic field (dynamo field of the Earth's outer core) and the atmosphere protect the Earth's surface from the solar wind (creating the external magnetic field). Outside the Earth's atmosphere the shielding by the atmosphere is absent and therefore the external magnetic field is very strong; this can lead to a failure of satellite function and therefore could cause serious problems for essential telecommunication systems (so the “space weather” has to be monitored).



Parameters of the Earth magnetic field at point P

- I - inclination
- D - declination
- T - total field ($T^2 = H^2 + Z^2 = X^2 + Y^2 + Z^2$)
- Z - vertical (downward) component of T
- X - component of T in geographic North direction
- Y - component of T in geographic East direction
- H - horizontal component of T

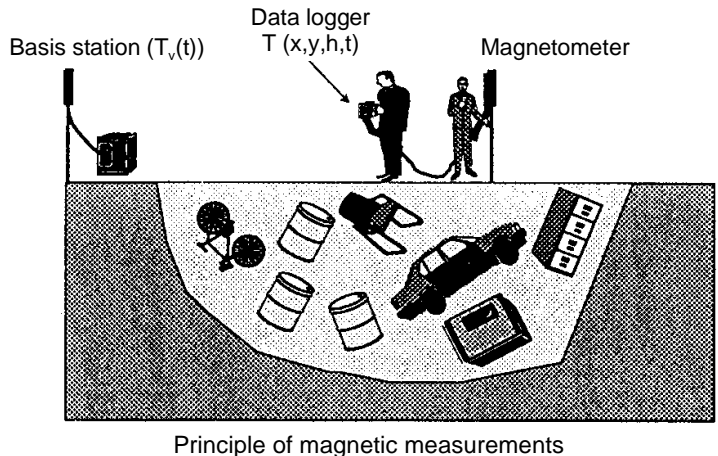
C.2 Magnetic field measurements and their interpretation

In most cases the total intensity T is measured by

- proton precession magnetometer (sensitivity 0.1 nT; Overhauser magnetometer 0.01 nT)
- optically pumped magnetometer (sensitivity 0.01 nT and better)

Components can be measured by

- fluxgate magnetometer (sensitivity 0.1 nT)



Measured total intensity: $|\vec{T}| = |\vec{T}_0(x,y) + \vec{F}(x,y) + \vec{T}(t)|$

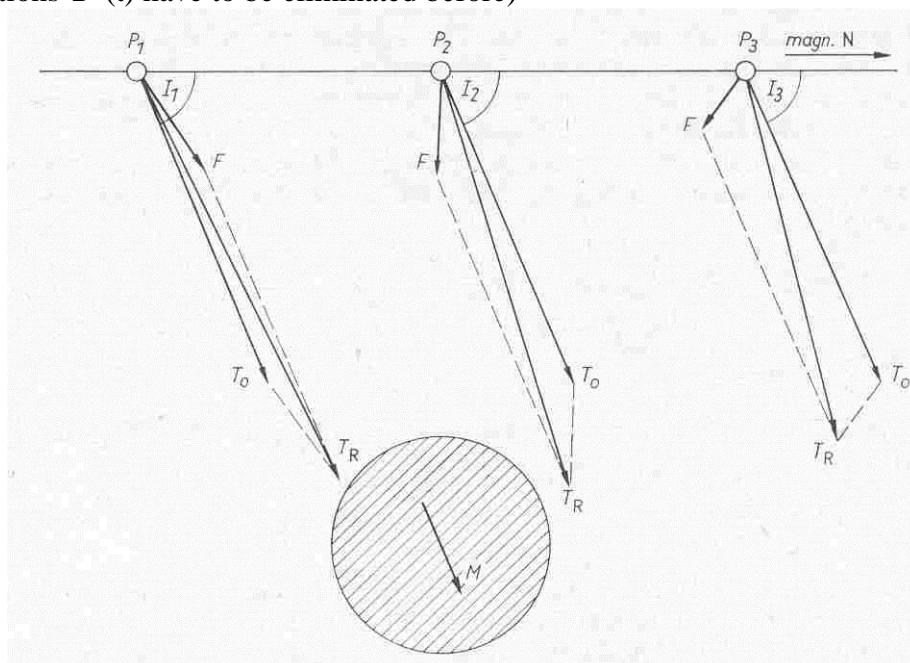
$\vec{T}_0(x,y,t)$ - Earth magnetic field (including time variation)

$\vec{F}(x,y,h)$ - magnetic field caused by the magnetized subsurface structure

$\vec{T}(t)$ - time-dependent variations (Earth magnetic field; instrument drift)

The total field anomaly δT is $|\vec{T}_0(x,y) + \vec{F}(x,y)| - |\vec{T}_0(x,y)|$

(time variations $\vec{T}(t)$ have to be eliminated before)



Vector addition of the field of anomaly and the Earth magnetic field

Magnetic measurements are fast (few seconds per measurement or even quasi-continuous) and are therefore being mostly done in a dense spatial grids.

A base station is used to correct for time variations. Often the field of anomaly F is high compared to T(t) and then such correction is not necessary.

Correction for the global field of the Earth is usually not required as the field anomaly is almost generally high against spatial variations of the Earth magnetic field in the measurement area (measurement areas are mostly in the order of 100 m, except for aeromagnetic surveys).

Topographic effects can be avoided by keeping some distance from steep topographic positions.

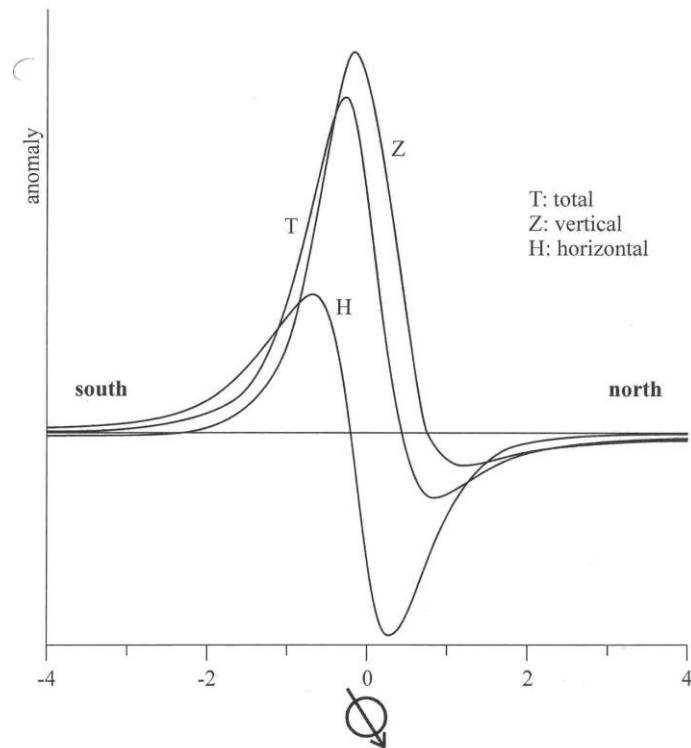
The **shape of the anomaly** depends on

- where on the globe it is measured
- in which profile direction it is measured
- which component is measured (total field T, vertical comp. Z, horizontal comp. H)
- the direction of magnetization (M_i or M_r or the vector sum of both)

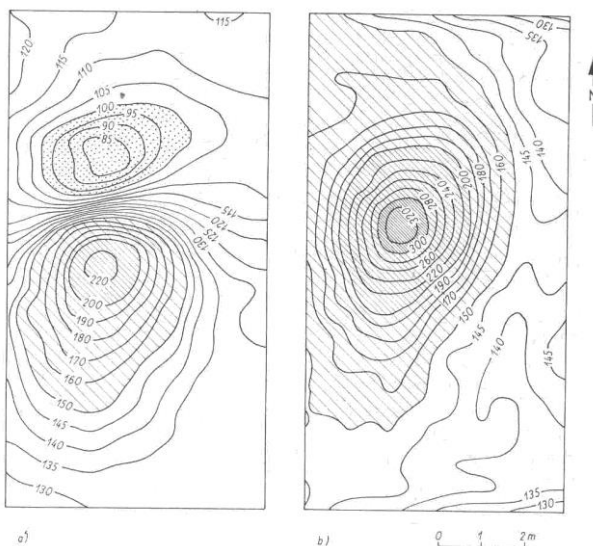
Note: magnetic anomalies usually have both maximum and minimum (different from gravity)

Similar to gravity the maximum depth t_{\max} can be estimated by the **half-width HW** or, alternatively, by the **distance of maximum and minimum Max-Min** (rule of thumb: use Max-Min if the magnitude of max. and min. differ by less than a factor of 2, otherwise use HW).

$$t_{\max} \approx \text{HW} \quad \text{or} \quad t_{\max} \approx \text{Max-Min}$$



Magnetic anomaly on a N-S profile for induced magnetization at moderate northern latitude.

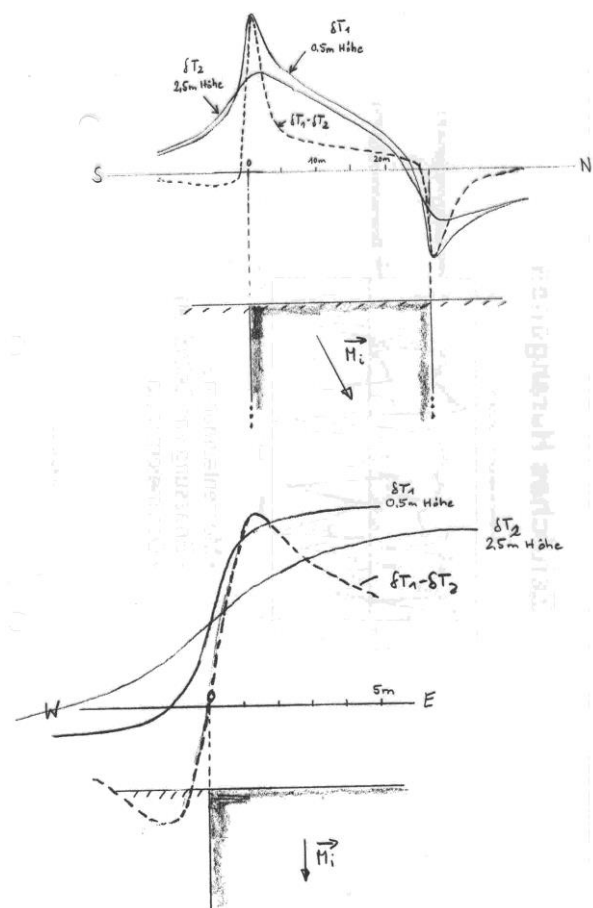


(left side) measured anomaly of an induced magnetisation; (right side) anomaly after pole reduction (= anomaly how it would like when the same subsurface structure would have been measured at the pole)

“Gradient” measurements can help to better identify lateral boundaries of bodies (difference of signals measured at two different heights above ground)

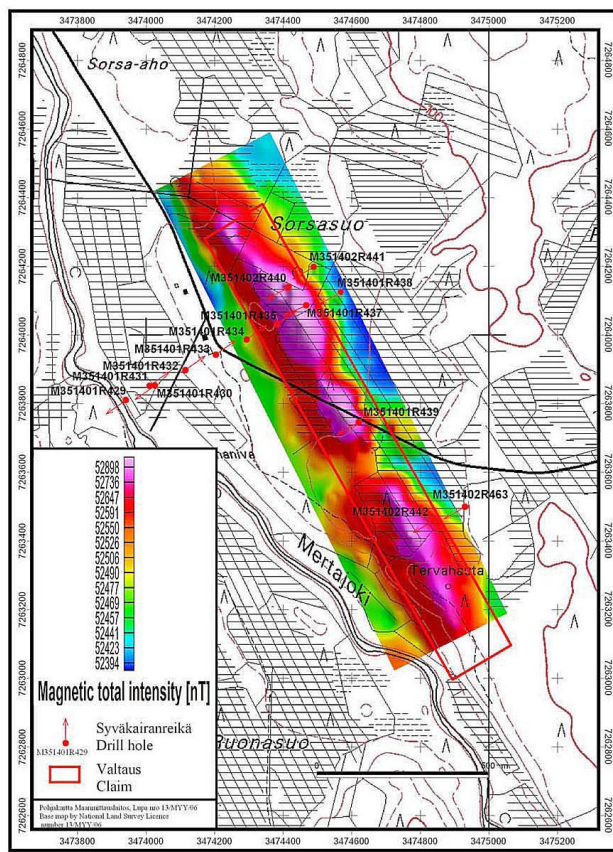
This is an efficient method when the body extends to larger depths, otherwise there is no significant improvement compared to measurement in only one level.

Note: Very shallow bodies can be usually easily detected by a complex shape of anomalies.
The boundaries of shallow bodies can be usually easily detected.

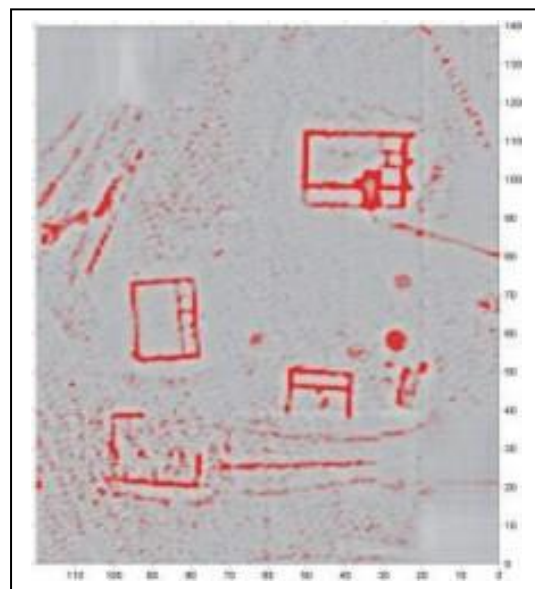


Schematic results of vertical gradient measurements

C.3 Examples for magnetic anomalies

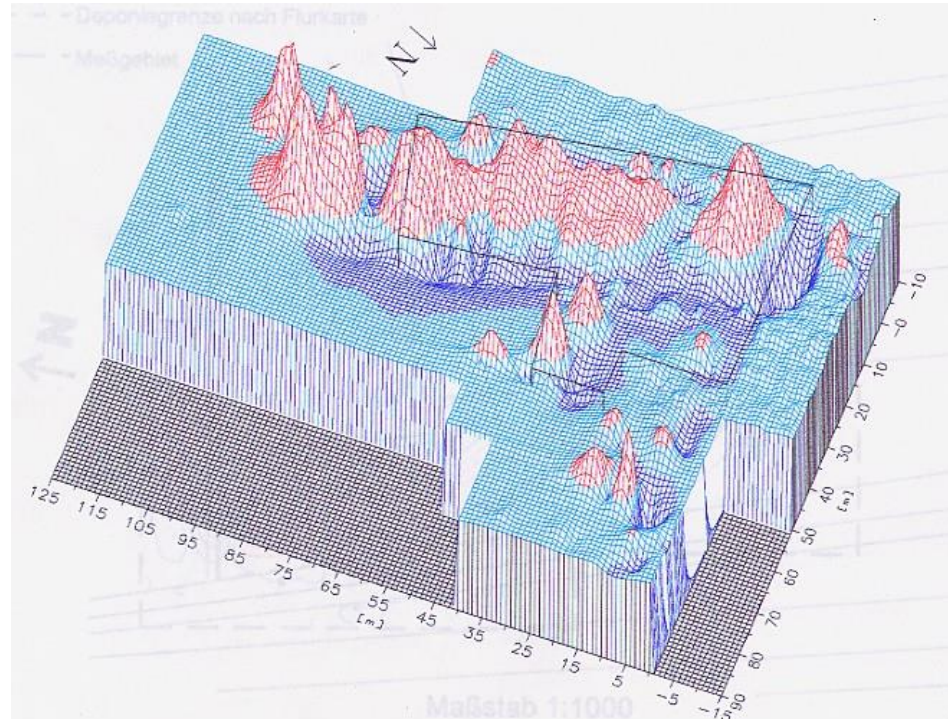


Magnetic map of the Sorsasuo area (From Juopperi & Karvinen, 2006).



(right side) Archaeological prospection with magnetic δT anomaly: wall relicts of ancient buildings very close to surface (anomalies are only a few nT)

(left side) Aeromagnetic mapping (δT) for the purpose of copper prospection



Magnetic anomaly (δT) over a re-cultivated former waste disposal site – the waste body is located below the soil horizon and extends down to few meters depth (anomalies are large: several 100 nT)

C.4 Nuclear magnetic resonance (NMR)

A radiowave source is used ($10^3 - 10^8$ MHz)



Precession of protons



Precession signal decays with characteristic relaxation times

NMR is used in medicine for tomography known as magnetic resonance tomography MRT (discriminating between fat and water)

For geotechnical applications NMR is used to measure the free water content (protons of H₂O)

C.5 Environmental magnetism

In environmental magnetism magnetic properties are used as (magnetic) proxies.

Magnetic proxy means: magnetic parameter which has a relationship to environmental conditions such as

- palaeoclimate or palaeoenvironment
- mass transport (e.g. where do sediments in a certain basin come from)
- anthropogenic pollution (in soil, sediment, air)

Such approach by using magnetic results is suitable when the magnetic parameter can be measured faster and cheaper than by more direct indicators. Often magnetic susceptibility is used because it can be measured extremely fast and very accurately.

Example 1: Heavy metals from industrial sources

Magnetic proxy mapping can be used as a low-cost tool for first-order determining contaminated areas. Magnetic particle content in soil, sediments and air may be linked to anthropogenic heavy metal (HM) contamination because HM and magnetic particles have the same sources (metallurgic industry, combustion, traffic, mining materials) and are transported in a similar way into the environment (transport by air & water).

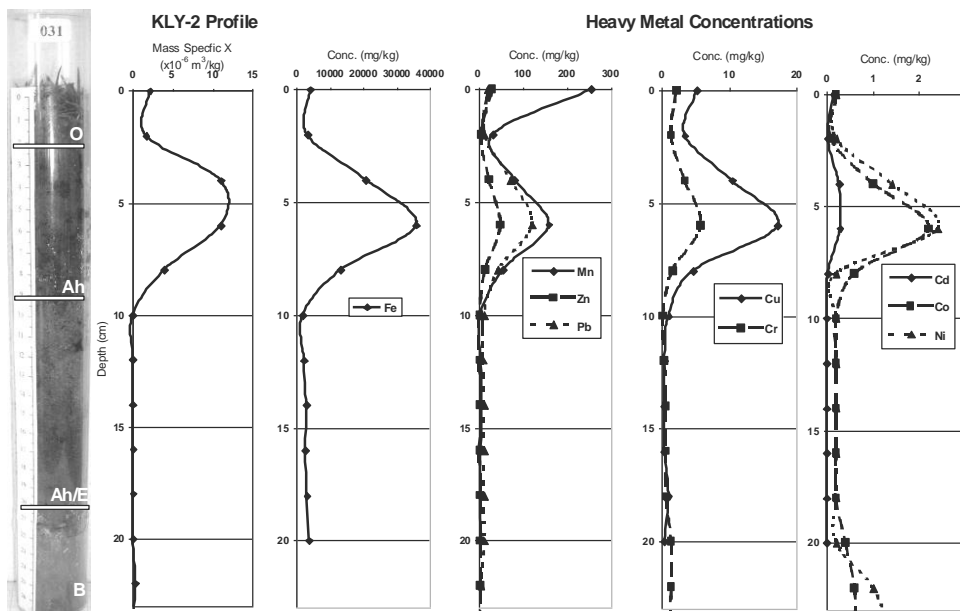
In many cases anomalous magnetic patterns correlate with areas of anthropogenic influence making the method effective for:

- quickly delineating potentially polluted areas
- monitoring long-term changes

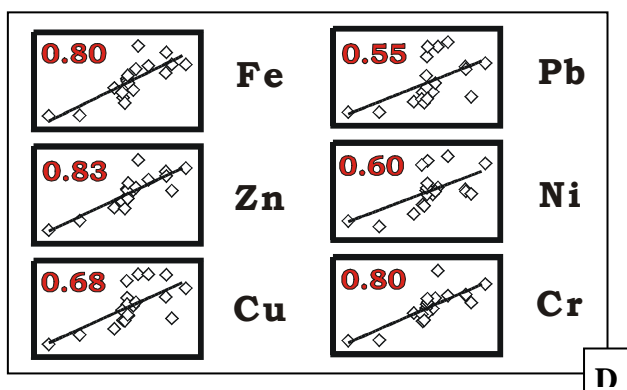
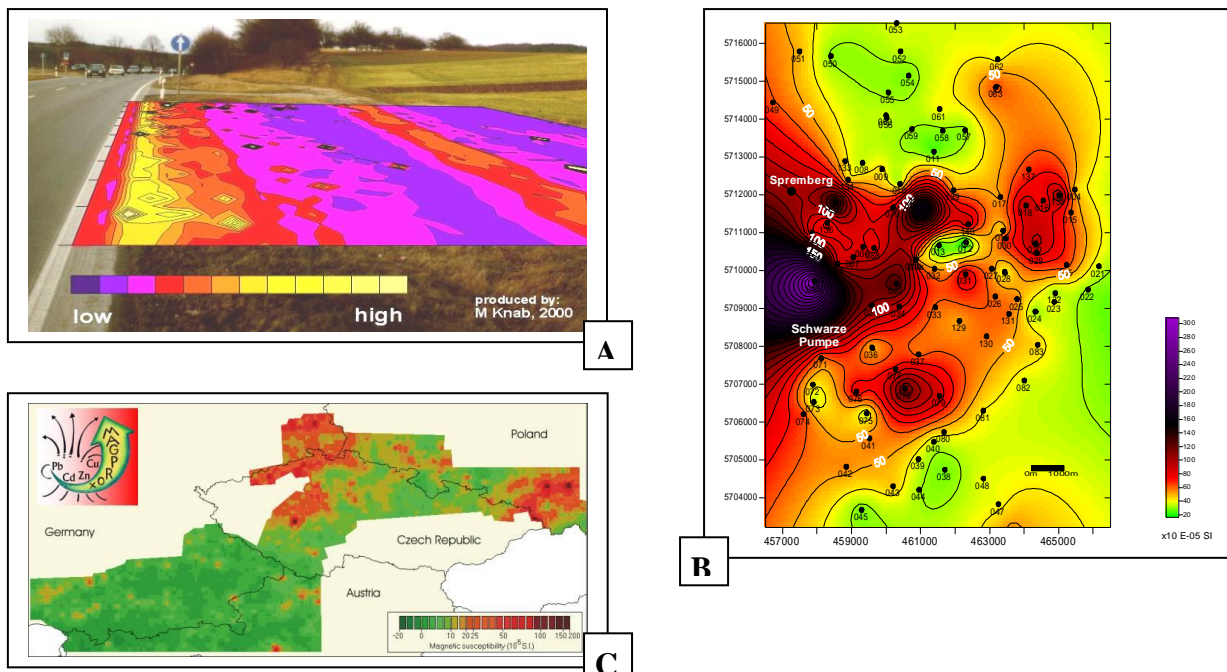
Magnetic proxies cannot determine the content of contaminants quantitatively – also they do not allow discriminating between different contaminants. However, information from magnetic proxy mapping allows a better selection of sites for chemical sampling.

Magnetic proxy measurements can be done

- on samples in laboratory
- in situ on surface (integral information about the uppermost ~10 cm)
- in situ on vertical sections (logging)



Magnetic susceptibility in a shallow vertical section (measured on samples) and heavy metal contents from the same samples

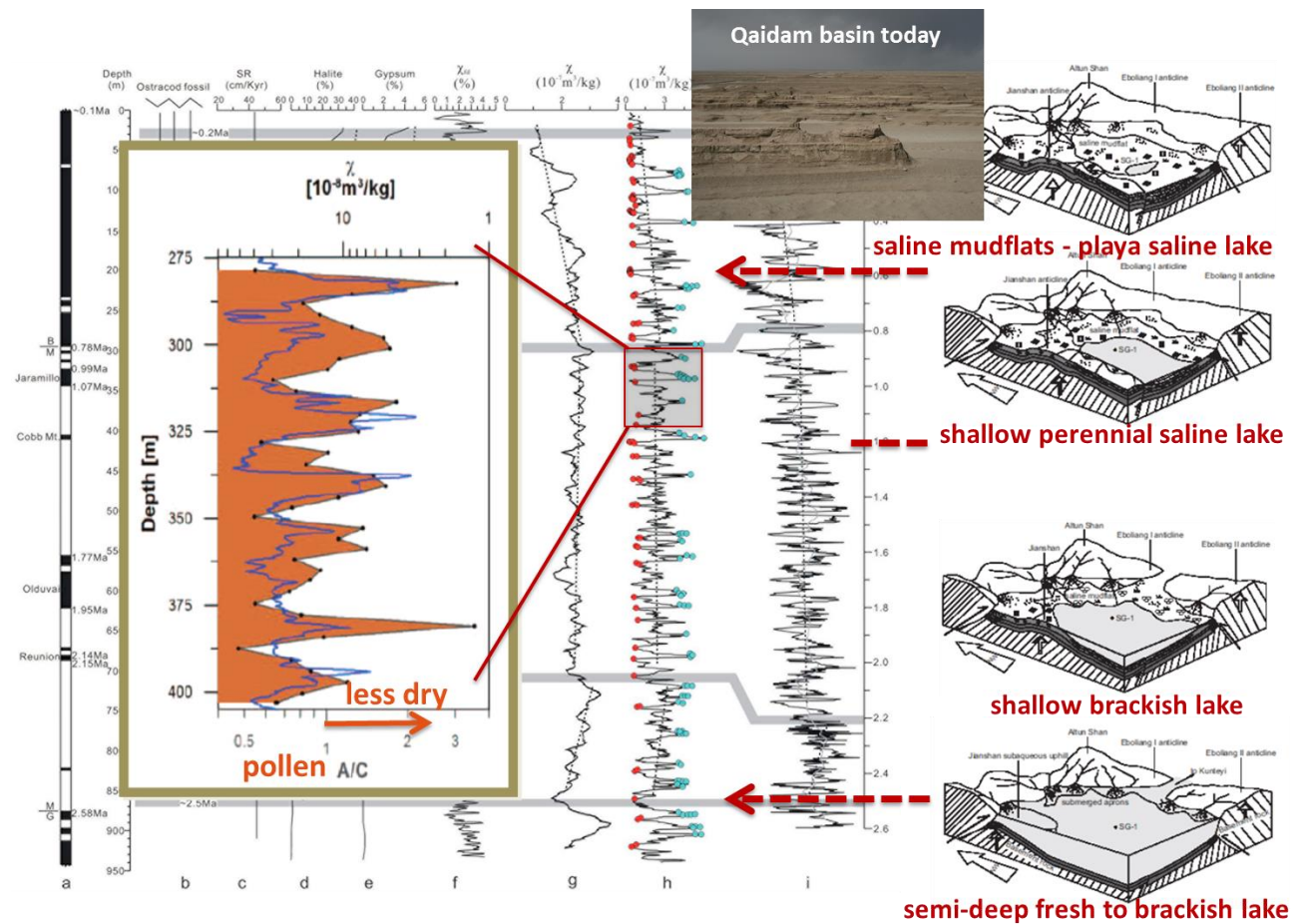


Examples for magnetic proxy screening:
 Magnetic susceptibilities measured in situ on surface for (A) roadside near Tübingen, (B) around a coal burning power plant in Germany, (C) large scale area across Europe.
 (D) Correlation (r) of magnetic susceptibility with heavy metals from dust accumulated on leaves at ring road of Kathmandu city.

Example 2: Palaeoclimate

The large desert zone in inner Asia (Taklamakan to Gobi desert) north of the Tibetan Plateau has a long geological history of drying (40 million years ago there was the large Paleotethys Sea, since then the Tibetan Plateau was growing and global climate was cooling with frequent oscillations) – how was the evolution of this aridification and what are the driving forces?

Iron minerals are very sensitive to climate conditions and therefore magnetic parameters may serve as proxies for palaeoclimate.



Example from a sedimentary sequence of the former lake in the Qaidam basin (north-eastern Tibetan Plateau). The figure shows results from a 940 m deep drill-core displaying the palaeoclimate evolution during drying of the basin since ca. 2.8 million years. Magnetic susceptibility (χ) shows high-amplitude fluctuations and the correlation with pollen data reveals that higher values of χ reflect drier conditions. Note that within one day one can measure χ values of more than thousand samples per day but can only analyze a few pollen samples.

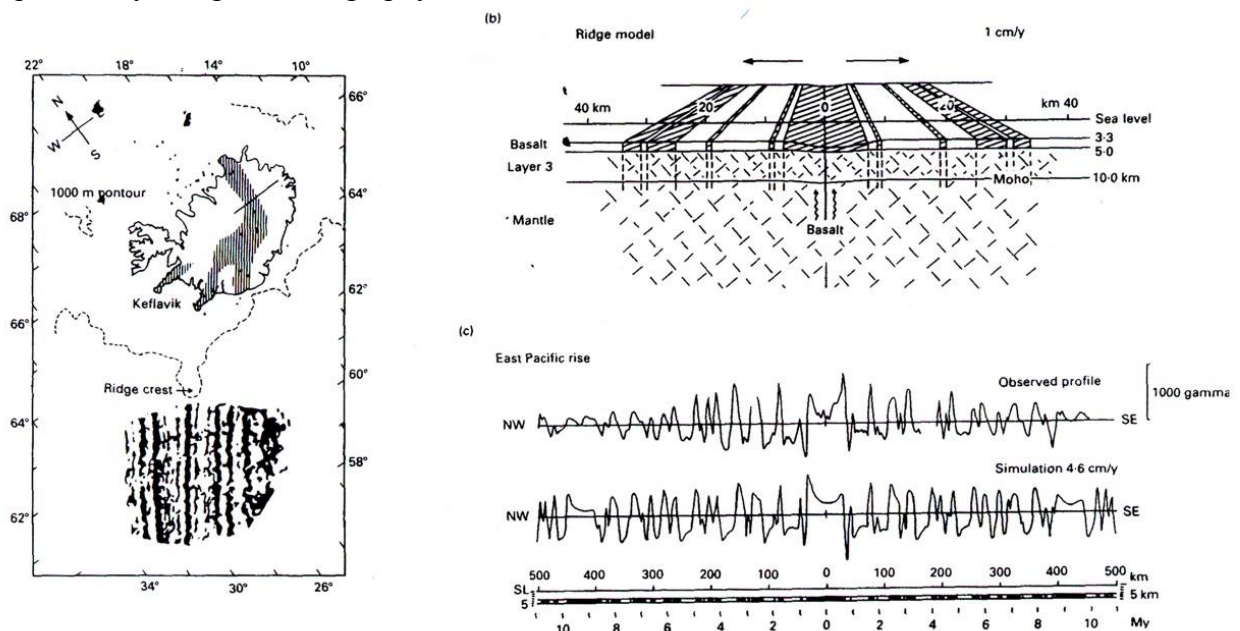
C.6 Palaeomagnetism

The Earth magnetic field magnetizes rocks during their formation (thermo-remanent magnetization in magmatic rocks, detrital remanent magnetization in sedimentary rocks). The acquired remanent magnetization is parallel to the Earth magnetic field and can be preserved for geological times in favourable cases (even for more than a billion years). It provides us information about the Earth magnetic field in the past. Acquisition of a remanent magnetization in the Earth's magnetic field and its recovery by sensitive magnetometers in the laboratory is comparable to saving data on a hard-disk and reading it from the disk later.

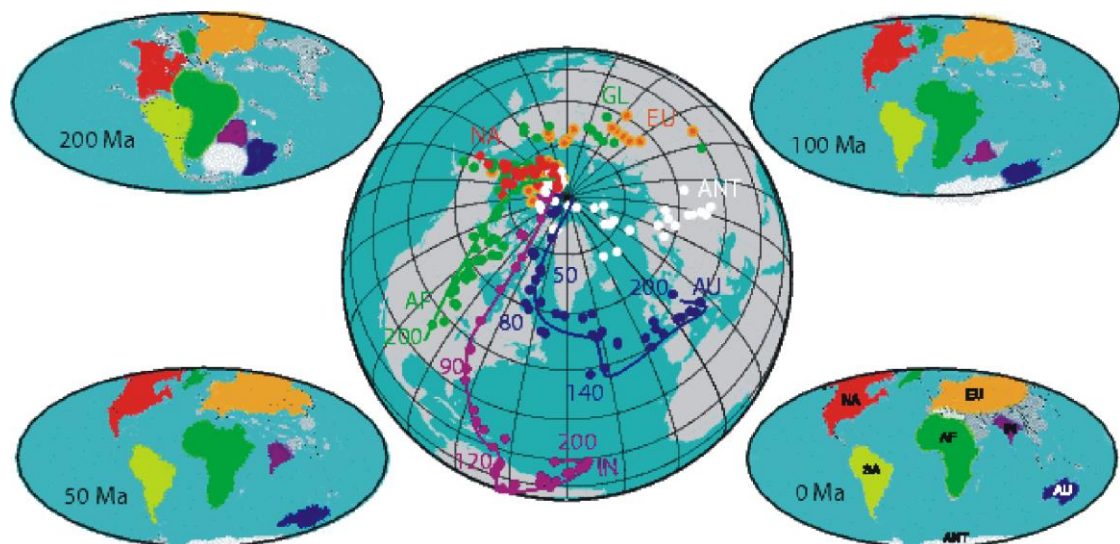
This remanent magnetization can be used to quantitatively reconstruct continental drift and also to decipher the kinematics of crustal deformations in orogens (north-south movements and rotations around a vertical axis can be detected, but no east-west movements). For all major lithosphere plates so-called apparent-polar-wander-paths (APWP) have been established. An ‘apparent pole’ (or also called ‘virtual geomagnetic pole’) is derived from the measured remanent magnetization with the assumption of a dipole field. Note that not the magnetic pole position has changed but the plates have moved – APWPs are just a convenient tool to describe these plate movements.

Such plate movement reconstructions require the validity of the hypothesis that within the geological past the Earth magnetic field (averaged on ca. 10.000 years) was always a dipole field with a dipole axis parallel to the Earth's rotation axis. The variation of the dipole field axis around an axial dipole (i.e. parallel Earth's rotation axis) is called ‘secular variation’.

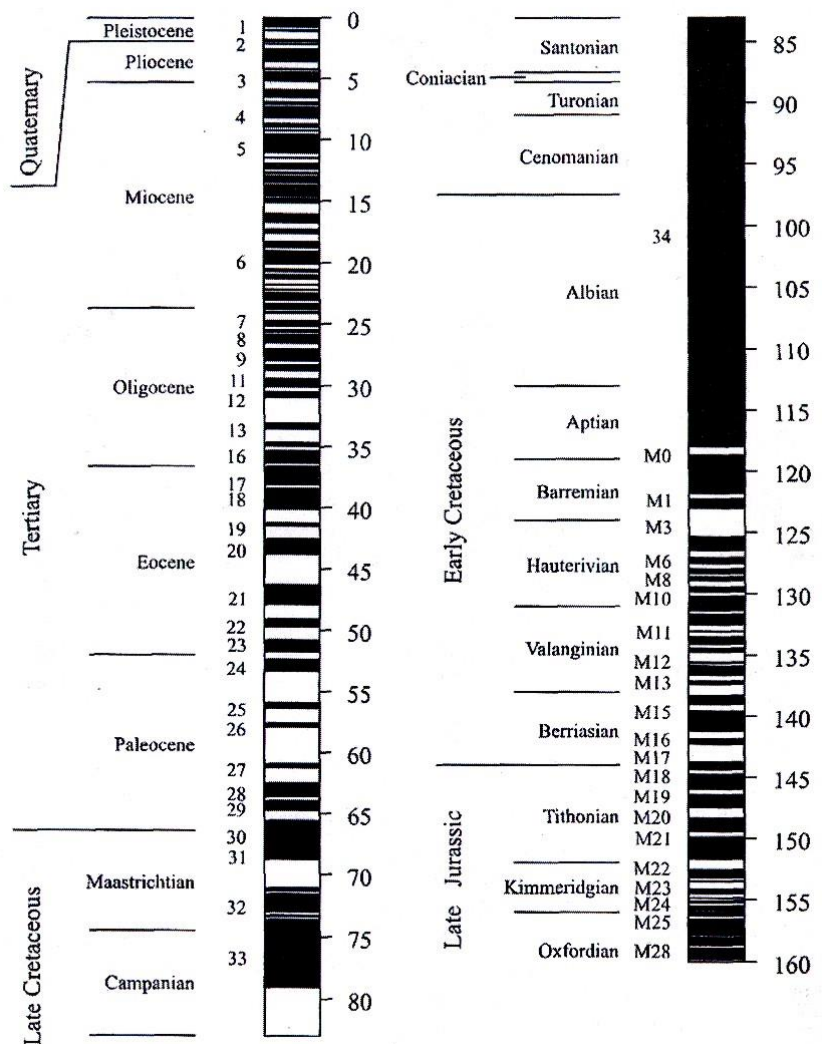
Polarity changes (“reversals”) of the Earth magnetic field have been detected by the remanent magnetization of the ocean floor basalts (magnetic “stripes”). These polarity changes occurred at very irregular periods. Temporal calibration of reversals allows dating of sedimentary sequences by “magnetostratigraphy”.



(Left) Pattern of magnetic anomalies across the mid-Atlantic ridge south of Island
 (Right side) Modelling of magnetic anomalies observed on a profile across a mid-oceanic ridge (East-Pacific Rise) – the model is based on 2D block models matching with the concept of sea-floor spreading



APWPs of the major lithosphere plates and continental reconstruction for different geological times



Standard polarity-time scale of Earth magnetic reversals during the last 160 million years

D Electrics and Electromagnetics

D.1 Fundamentals

D.1.1 Parameters

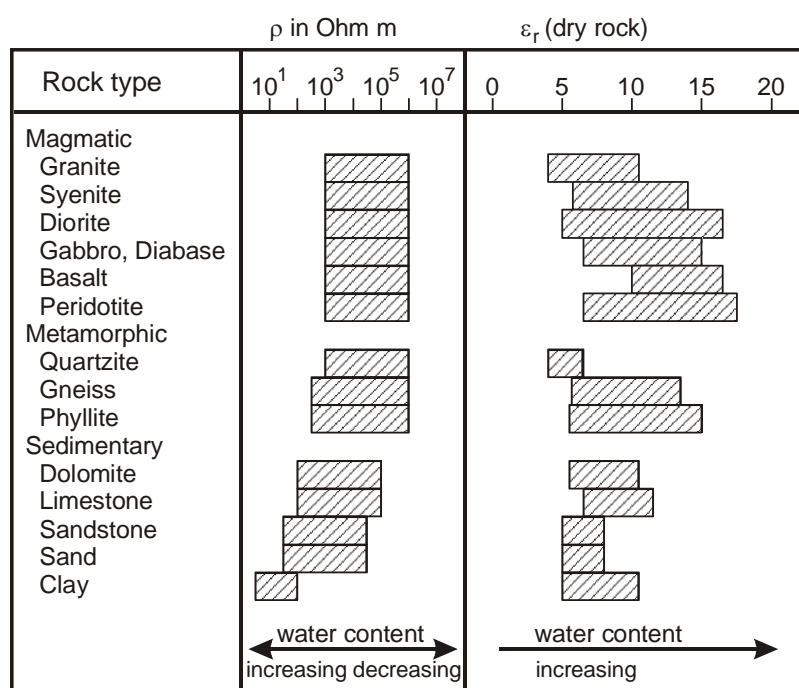
resistivity ρ [Ωm] and electrical conductivity σ [Sm^{-1}]; $\rho = 1/\sigma$

dielectric permittivity $\epsilon = \epsilon_r \epsilon_0$ [$\text{A s V}^{-1}\text{m}^{-1}$], magnetic permeability $\mu = \mu_r \mu_0$ [$\text{V s A}^{-1}\text{m}^{-1}$]

ϵ_r relative electrical permittivity, $\mu_r = 1 + \kappa$ relative magnetic permeability

$\epsilon_0 \approx 8,854 \cdot 10^{-12} \text{ AsV}^{-1}\text{m}^{-1}$ electrical permittivity in free space

$\mu_0 = 4\pi \cdot 10^{-7} \text{ VsA}^{-1}\text{m}^{-1}$ magnetic permeability in free space



Mean value ranges of specific electrical resistivity and relative permittivity for some rock types (arrows indicate the tendency of changing with water content)

D.1.2 Mechanisms of electrical conduction

Ionic conduction

Moving ions in fluids; conductivity depends on the concentration of ions and pore space distribution (connection of pores) and increases with higher temperature (more dissolved ions, viscosity of the fluid lower)

Metallic conduction

Free electrons in the metal lattice; conductivity depends on the metal type and decreases with higher temperature (higher lattice oscillations)

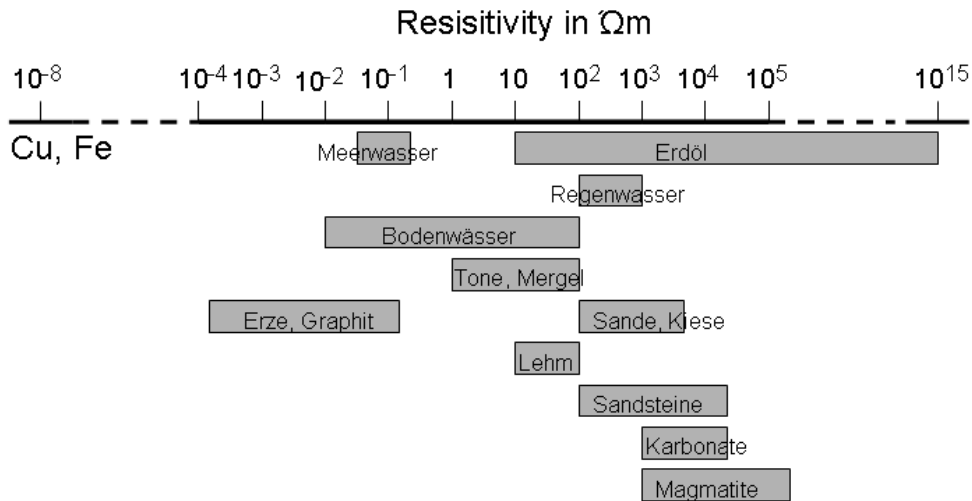
Semi-conduction

Electrons in the conduction band; conductivity depends on the material and increases with temperature (more electrons in the conduction band)

Clay minerals have a relatively high conductivity because of their negative surface charges (surface charges bind positive ions from the fluids around) – this creates a special kind of ionic conduction.

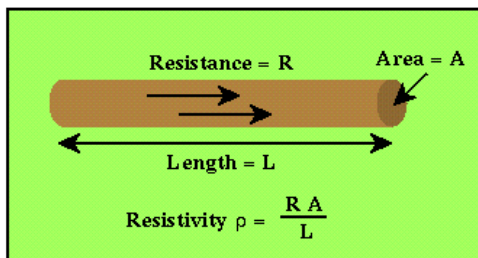
In shallow subsurface and also in most parts of the Earth's crust ionic conduction is the determining mechanism
(only in ore deposits or graphite layers metallic conduction becomes important).

In the Earth's mantle increased temperature leads to dominance of semi-conduction (ca. $40 \Omega\text{m}$ in 400 km depth, ca. 1 to $0.1 \Omega\text{m}$ near the mantle-core boundary).



Erdöl = raw oil, Meerwasser = sea water, Regenwasser = rain water, Bodenwässer = groundwater, Erze = ores, Graphit = graphite, Tone = clays, Mergel = marls, Sande = sands, Kiese = gravels, Sandsteine = sandstones, Karbonate = carbonates, Magmatite = magmatic rocks

The fundamental electrical property is *resistivity*, not *resistance*



Resistivity is a material property

Resistance depends on the measurement configuration and the material property

Archie's laws: $\rho_{100} = F \cdot \rho_w$; $F = a \cdot \Phi^{-m}$;

$$\text{for partial saturation: } (S_w)^n = \frac{\rho_{100}}{\rho}$$

a, m, n are empirical constants, they vary especially for different rock types (e.g. sandstone, carbonates)

ρ_{100} - resistivity of 100 % saturated rock, ρ_w - resistivity of pore fluid, Φ ($0 \leq \Phi \leq 1$) - porosity, S_w ($0 \leq S_w \leq 1$) - saturation degree, ρ - resistivity of rock

The formulas above are only valid for clay-free materials.

For materials containing clays it has to be extended to: $\frac{1}{\rho} = \frac{1}{\rho_{clay}} \cdot S_{clay} + \frac{\Phi^m}{a \cdot \rho_w} \cdot S_w^2$

D.1.3 Maxwell equations

Four Maxwell equations together with the Ohm's law and two material equations are the fundamental equations of electromagnetism.

The **Maxwell equations** can be written in operator or integral form. For calculations the easier one can be used (depends on the given case).

The first two equations describe electric and magnetic field phenomena separately (static fields), while the other two describe effects of electric and magnetic field interaction.

$$\operatorname{div} \vec{B} = 0 \quad \text{or} \quad \oint \vec{B} \cdot d\vec{F} = 0$$

$$\operatorname{div} \vec{D} = q_v \quad \text{or} \quad \oint \vec{D} \cdot d\vec{F} = Q$$

$$\operatorname{curl} \vec{H} = \vec{j}_c + \frac{\partial}{\partial t} \vec{D} \quad \text{or} \quad \oint \vec{H} \cdot d\vec{s} = \int \left(\vec{j}_c + \frac{\partial}{\partial t} \vec{D} \right) d\vec{F} \quad (\text{Ampère's law})$$

$$\operatorname{curl} \vec{E} = -\frac{\partial \vec{B}}{\partial t} \quad \text{or} \quad \oint \vec{E} \cdot d\vec{s} = -\frac{\partial}{\partial t} \int \vec{B} \cdot d\vec{F} \quad (\text{Faraday's law or induction law})$$

$$\vec{j} = \sigma \cdot \vec{E} \quad \text{Ohm's law} \quad (\vec{j} = \vec{j}_c + \vec{j}_D)$$

$$\vec{D} = \epsilon_r \epsilon_0 \vec{E} \quad \vec{B} = \mu_r \mu_0 \vec{H} \quad \text{material equations}$$

\vec{E} : electric field, \vec{D} : dielectric field

\vec{H} : magnetic field, \vec{B} : magnetic induction

\vec{j}_c : conduction current density;

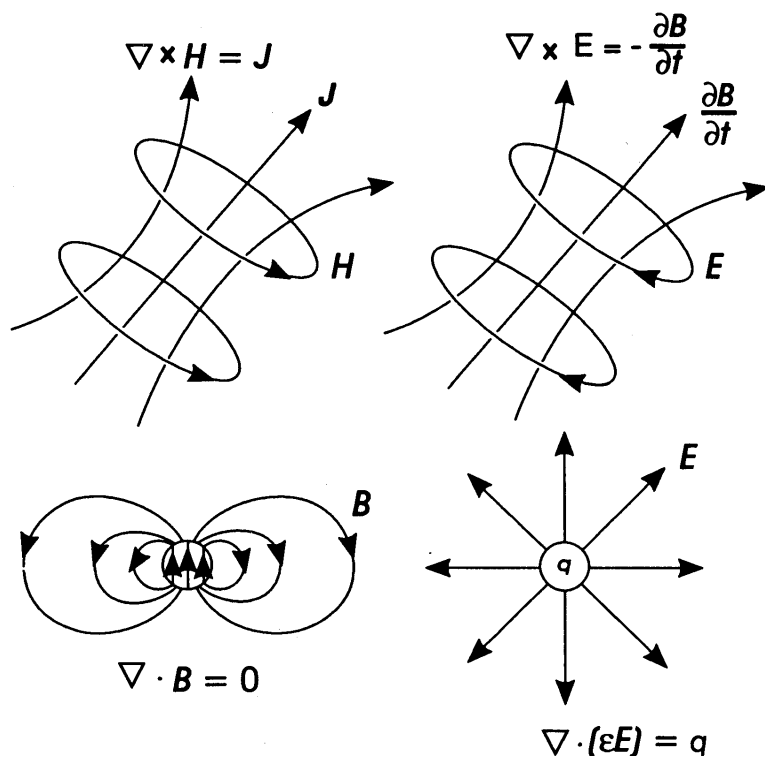
$\vec{j}_D = \frac{\partial}{\partial t} \vec{D} = \epsilon \frac{\partial}{\partial t} \vec{E}$: displacement / dielectric current density

q_v : electrical charge density, Q : electrical charge

ϵ : dielectric permittivity, μ : magnetic permeability

Operators div , grad , curl :

$$\operatorname{div} = \nabla \cdot = \frac{\partial_x}{\partial x} + \frac{\partial_y}{\partial y} + \frac{\partial_z}{\partial z} \quad \operatorname{grad} = \nabla = \begin{pmatrix} \frac{\partial}{\partial x} \\ \frac{\partial}{\partial y} \\ \frac{\partial}{\partial z} \end{pmatrix} \quad \operatorname{curl} = \nabla \times = \begin{pmatrix} \frac{\partial_z}{\partial y} - \frac{\partial_y}{\partial z} \\ \frac{\partial_x}{\partial z} - \frac{\partial_z}{\partial x} \\ \frac{\partial_y}{\partial x} - \frac{\partial_x}{\partial y} \end{pmatrix}$$

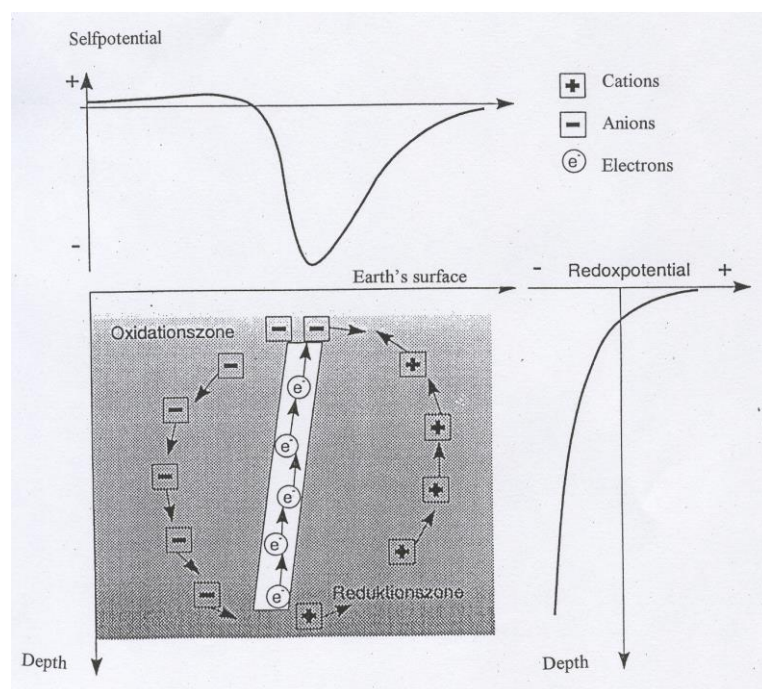


Meaning of Maxwell equations

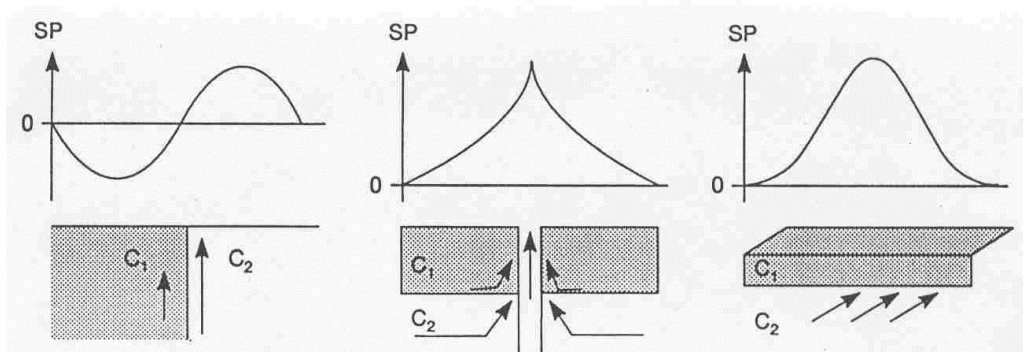
D.2 Self Potential (Spontaneous Potential) method

Self potentials arise from:

1. Redox-potential
2. Contact potential (diffusion potential)
3. Filtration potential (flow potential)

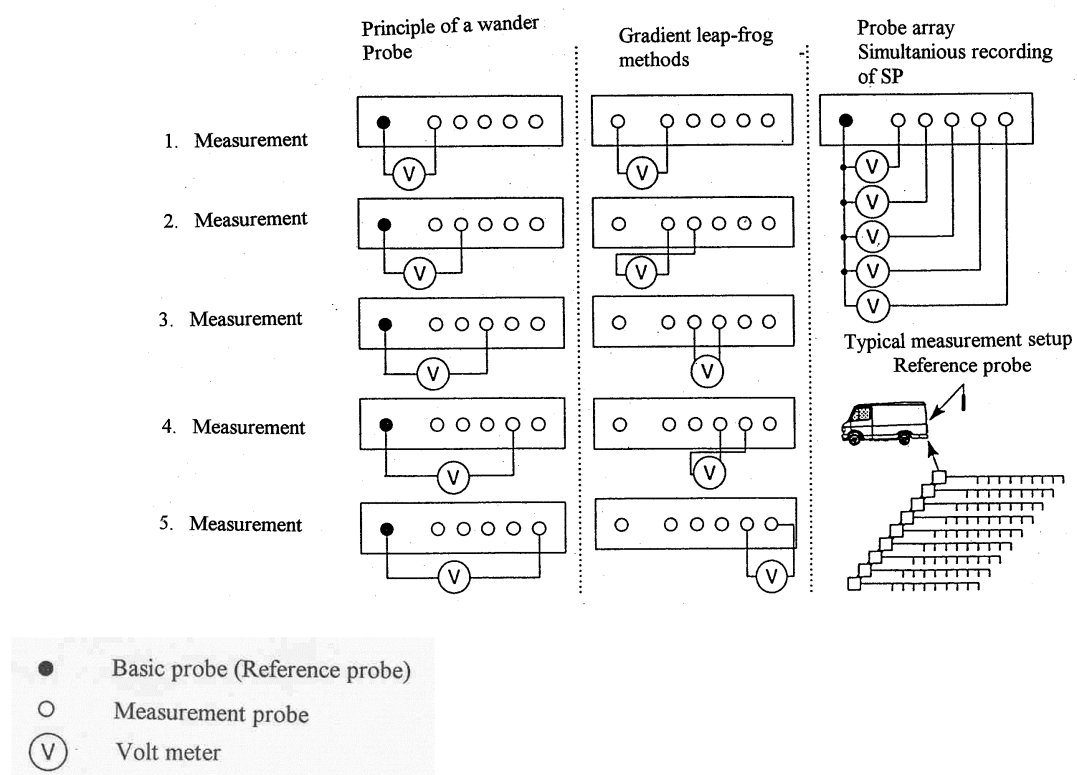


Self potential anomaly related to redox processes

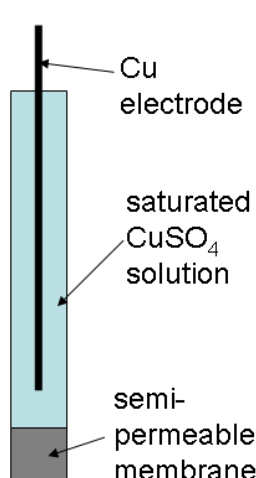


→ flow directions, C_1 & C_2 - flow potential coefficients

Flow potential anomalies induced by fluid flow at boundaries between materials with different flow potential coefficients



Measurements have to be done with **unpolarizable electrodes** to avoid strong contact potential between metal and pore fluid.



D.3 DC – Geoelectrics

D.3.1 Fundamental equations

Force F between two charges q and Q at distance of r :

$$F = \frac{1}{4\pi\epsilon_0} \frac{q \cdot Q}{r^2} = q \cdot E$$

Coulomb law

$$E = \frac{1}{4\pi\epsilon_0} \frac{Q}{r^2} \quad \text{electric field created by } Q ; \quad V = \frac{1}{4\pi\epsilon_0} \frac{Q}{r} \quad \text{electric potential due to } Q$$

$$\vec{E} = -\operatorname{grad}V \quad (F, E, j \text{ are vectors, while } V \text{ is a scalar})$$

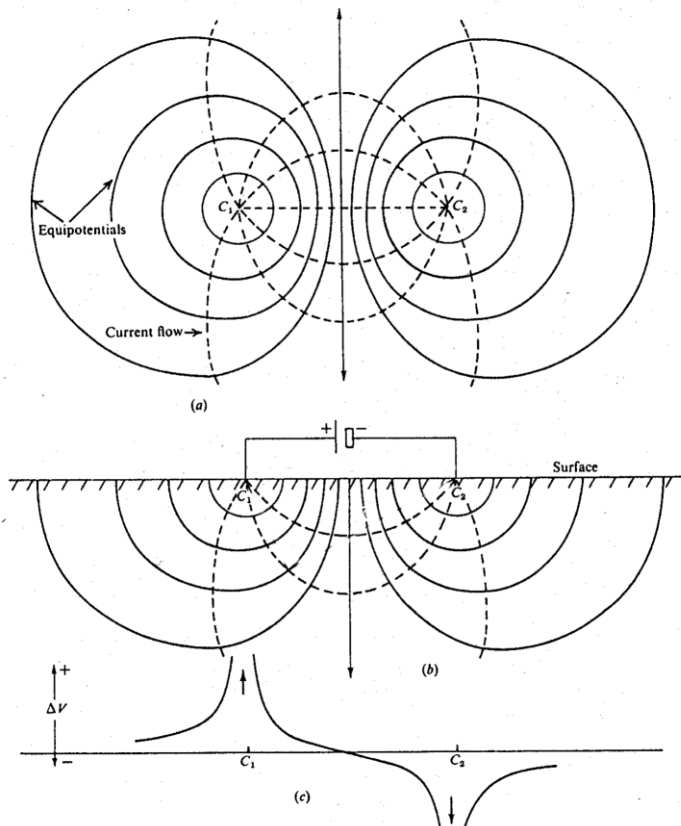
The Coulomb law is valid for charges in free space (more generally: in non-conductive space). If a charge is connected to a conductive medium a current flow arises which is described by the Ohm's law $\vec{j} = \sigma \cdot \vec{E}$

For the electric potential of a point source in homogeneous media we get:

$$\text{in full space} \quad V(r) = \frac{I}{4\pi\sigma} \cdot \frac{1}{r} = \frac{\rho I}{4\pi} \cdot \frac{1}{r}$$

$$\text{in half space} \quad V(r) = \frac{I}{2\pi\sigma} \cdot \frac{1}{r} = \frac{\rho I}{2\pi} \cdot \frac{1}{r} \quad (\text{charge at surface})$$

(I – electric current injected by the source=charge, r - distance to source point)



- (a) surface view and (b) vertical section of current flow lines (equal to electric field lines) and equipotential lines ($V=\text{constant}$) for point sources C_1 (positive charge) and C_2 (negative charge) at surface
 (c) voltage ΔV (potential difference versus 0-potential) at the surface along a straight line passing through the point sources C_1 and C_2

D.3.2 The concept of 4-point array measurements

Surface measurements with just a 2-electrode configuration (as shown in the figure above in D.3.1) do not give meaningful results because the contact between current electrodes (C_1, C_2) and the ground may have a very high contact resistance.

To avoid this problem 4-point arrays are generally used: Injection of current I into the ground by current electrodes (usually termed A,B) and measurement of voltage ΔV between two additional electrodes (usually termed M,N) ($\Delta V = V_M - V_N$).

From the formula $V(r)$ in D.3.1 it follows:

$$\rho = K \frac{\Delta V}{I} \quad \text{with} \quad K = \frac{2\pi}{\left(\frac{1}{r_{AM}} - \frac{1}{r_{BM}}\right) - \left(\frac{1}{r_{AN}} - \frac{1}{r_{BN}}\right)}$$

K is called the configuration factor (or geometry factor), it depends on the geometrical setting of A,B,M,N positions.

For homogenous ground the result for ρ will be the true value of the ground.

For inhomogeneous ground the result for ρ will be an **apparent resistivity** termed as ρ_a (or ρ_s).

D.3.3 Different configurations of 4-point arrays

In principle all kinds of electrode geometries are possible but there are several common configurations for DC-geoelectrical surface measurements:

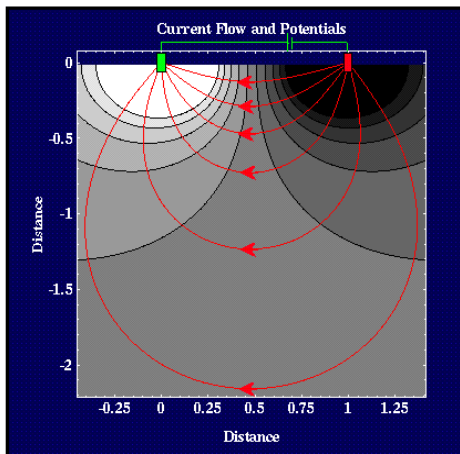
(current electrodes: A & A' - location of positive pole, B - location of negative pole; potential electrodes M,N; configuration factors are listed at the right side, respectively):

a)		$\frac{2\pi}{\frac{1}{r_{AM}} - \frac{1}{r_{AN}} - \frac{1}{r_{BM}} + \frac{1}{r_{BN}}}$	f)		$\pi a (n+1) (n+2)$
b)		$2\pi L$	g)		$\frac{\pi L (L^2+a^2)^{1/2}}{(L^2+a^2)^{1/2} L}$
c)		uncalculable	h)		$2a n (n+1) \pi$
d)		$\frac{2\pi L}{3}$	i)		$\frac{\pi L}{2} \quad (I_{\bar{A}} = I_A = L/2)$
e)		$\pi a n (n+1)$	j)		uncalculable $(I_{\bar{A}} = I_A = L/2)$

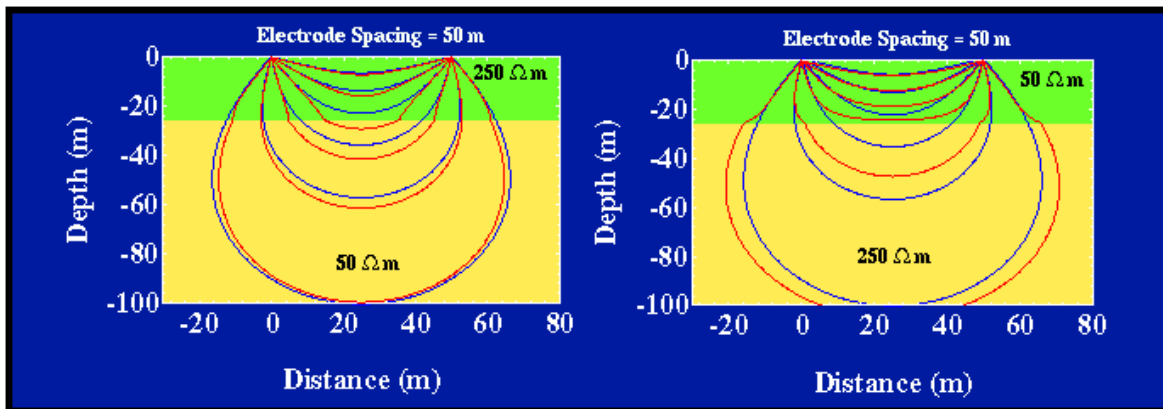
- a) General 4-point-configuration, b) Pole-Pole (or 2-Pole), c) Gradient, d) Wenner, e) Schlumberger, f) Dipole-Dipole, g) Equatorial Dipole-Dipole, h) Pole-Dipole (or 3-pole), i) focusing configuration type AMA', j) focusing configuration type AMNA'.

Note: there are different terminologies for electrode distances; e.g. for Wenner "a" instead of "L/3", for Pole-Pole "a" instead of "L", for Schlumberger "l" for AB and "s" for MN instead of "a(2n+1)" and "a".

D.3.4 Current distribution and signal contribution



Current path (from top to bottom)	% of total current
1	17
2	32
3	43
4	49
5	51
6	57



(top) Current distribution and equipotential lines in homogenous half space; the table shows how much % of the total current flows within the given current line (red lines).

(bottom) Current lines for a two-layer case (red lines), compared to the homogeneous ground cas (blue lines).

The **depth of penetration** is given by the electric current density as shown in the top figure above. For the depth of penetration only the setting of the A and B electrodes is important (and the resistivity structure of the ground).

But how much do different parts in the subsurface contribute to the measured ρ_s value? For this additionally the setting of the M and N electrodes counts.

The effect of a particular deviation in the ρ -distribution on the determined ρ_s -value within a distinct subsurface part (subvolume=cell) can be expressed by:

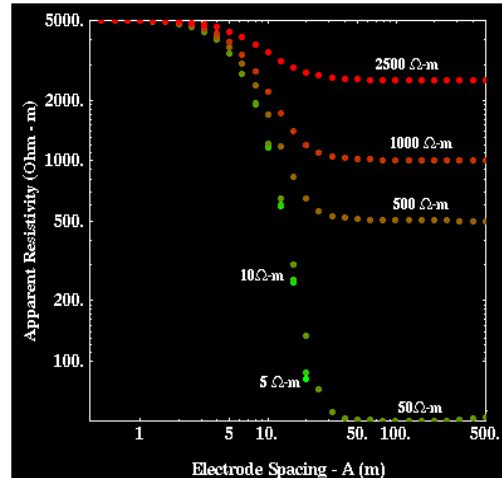
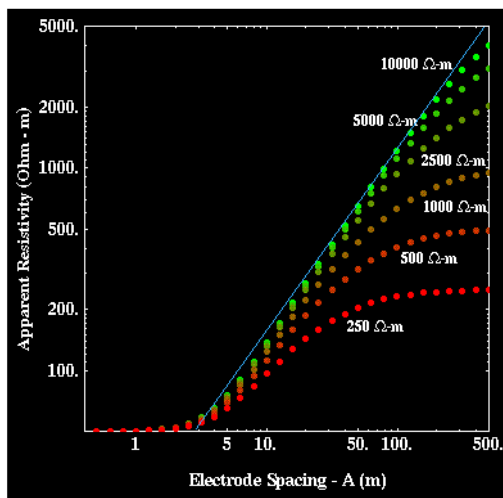
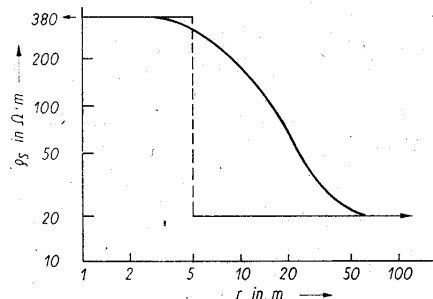
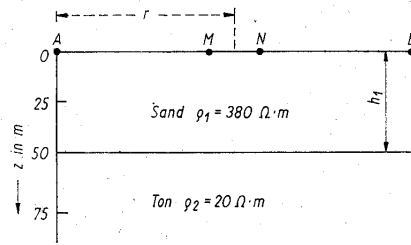
$$\Delta\rho_s = \sum_{j=1}^m S_j \cdot \Delta\rho_j$$

($\Delta\rho_j$: deviation of ρ in the j -th cell from the ρ -value in the homogeneous surrounding; S_j : sensitivitiy coefficient of the j -th cell; $\Delta\rho_s$: resulting deviation in the measured ρ_s -value , m – number of cells building up the whole subsurface).

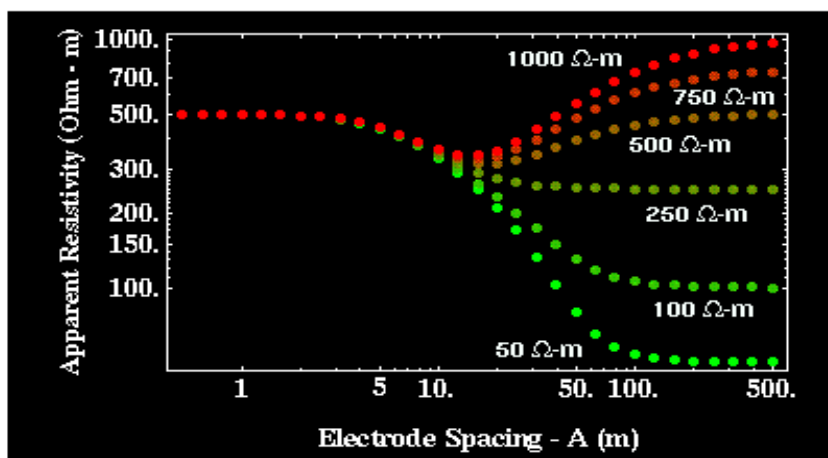
D.3.5 Vertical electrical sounding (VES)

For VES, ρ_s is measured for different electrode spacings with the array mid-point remaining fixed. Usually, a Schlumberger or Wenner array is used or VES.

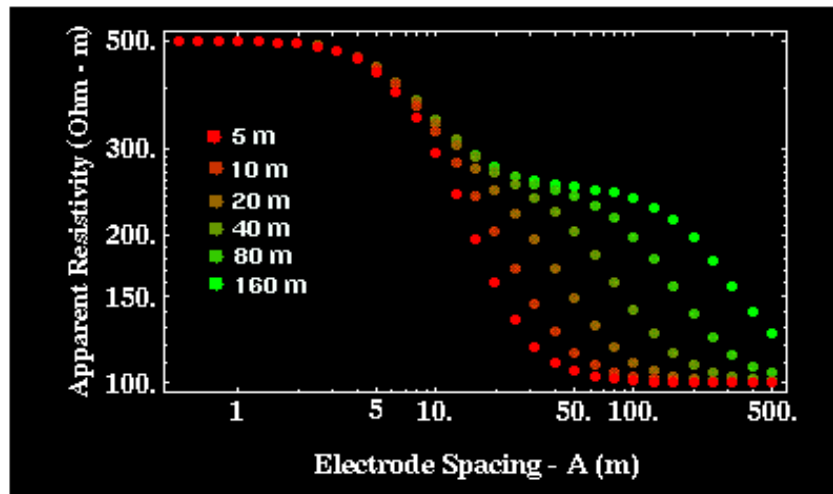
Results are plotted in a bi-logarithmic diagram of ρ_s versus electrode spacing r (e.g. $r=AB/2$ as for the Schlumberger example below) resulting in a ρ_s curve:



ρ_s curves for a two-layer case - with top layer: thickness 10 m, resistivity 50 $\Omega\text{-m}$ (left side) or 5000 $\Omega\text{-m}$ (right side)
different curves denote different bottom layer resistivities with values given in the figures



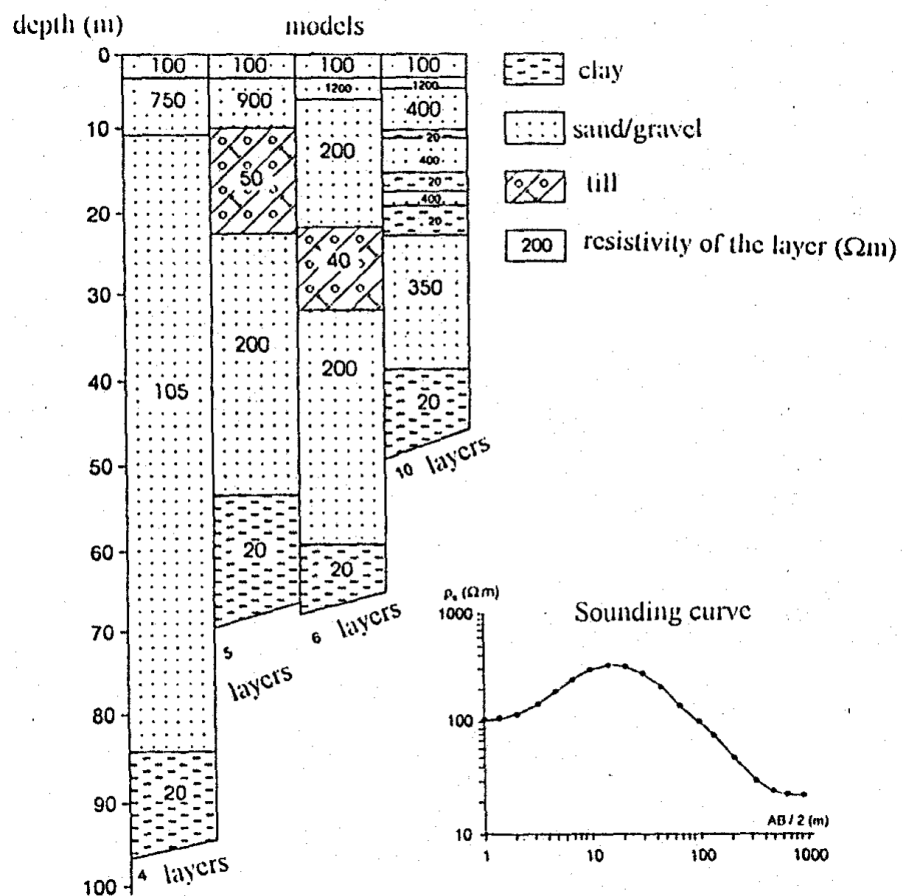
ρ_s curves for a three-layer case showing the influence of the resistivity of the third layer
top layer: 500 $\Omega\text{-m}$, 5 m thick; 2nd layer: 250 $\Omega\text{-m}$, 15 m thick; resistivity of the 3rd layer as shown in the figure



ρ_a curves for a three-layer case showing the influence of the thickness of the second layer
(top layer: 500 Ωm , 5 m thick; 2nd layer: 250 Ωm ; 3rd layer: 100 Ωm ; thickness of the 2nd layer as shown in figure)

There are several **ambiguities in the data inversion** leading to different models (see example below). In particular: the number of layers may be underestimated; a large range of “thin” intermediate layers can explain the data.

Before doing a 1D-inversion one also has to make sure that the data really represent a horizontal structure.



Equivalent models within 1.5% deviation for Schlumberger ρ_a curves

D.3.6 Depth of investigation (DOI) for VES

There are two alternative definitions:

(defined on sensitivity coefficients summed up over infinite thin horizontal planes)

a) Depth of maximum absolute sensitivity value

(Roy & Apparao, 1971)

b) Depth for which the sum of the sensitivity values of all 'layers' above is equal to the sum of the sensitivity values of all 'layers' below

(Edwards, 1977)

The DOI is dependent from the setting of all electrodes and it is different from the depth of penetration (i.e., the depth of the current penetration).

Signal contribution (y-axis) curves versus depth for

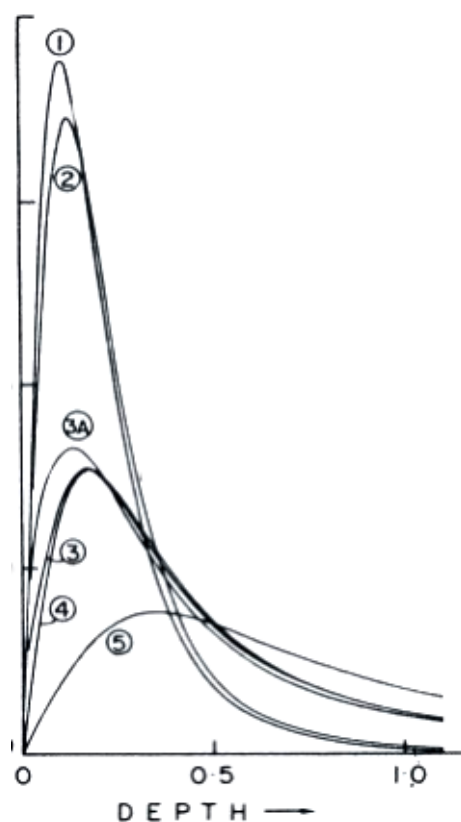
(1) Wenner array

(2) Schlumberger

(3,3A,4) different dipole-dipole arrays

(5) pole-pole array

The signal contribution value denotes sensitivity coefficients summed up over thin infinite layers; the depth axis is normalized to the electrode spacing L (L as defined in D.3.3)



Array type (L defined in D.3.3)	Depth of maximum signal contribution	Depth with equal signal contribution from above and below
Wenner	0.110 L	0.173 L
Dipole-dipole (high n)	0.195 L	0.250 L
Schlumberger	0.125 L	0.190 L
Pole-pole	0.350 L	0.867 L

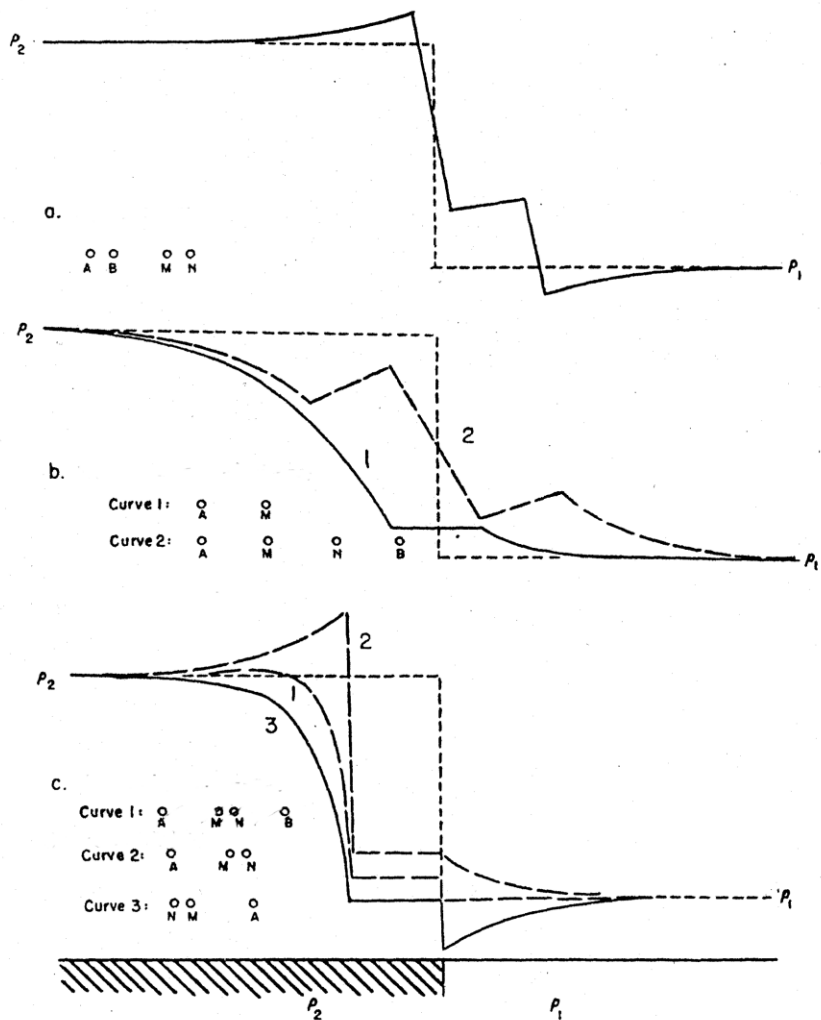
A narrow curve means good vertical resolution !!!!

As one can see from the figure above, the Schlumberger and Wenner arrays have the best vertical resolution, while depth resolution of the pole-pole array is poor. Therefore Wenner or Schlumberger are used for VES, but never Pole-Pole (Pole-Pole has advantages for profiling). The vertical resolution of Dipole-Dipole arrays (curves 3, 3A, 4 in the figure) is moderate, but it is suitable for combined VES and profiling (pseudosections – see further below).

D.3.7 Geoelectric Profiling and 2D-structures

For DC-geoelectrical profiling, the mid-point of the array is moved along a profile, measuring with one (1D-profiling) or more (2D-profiling) fixed electrode spacings.

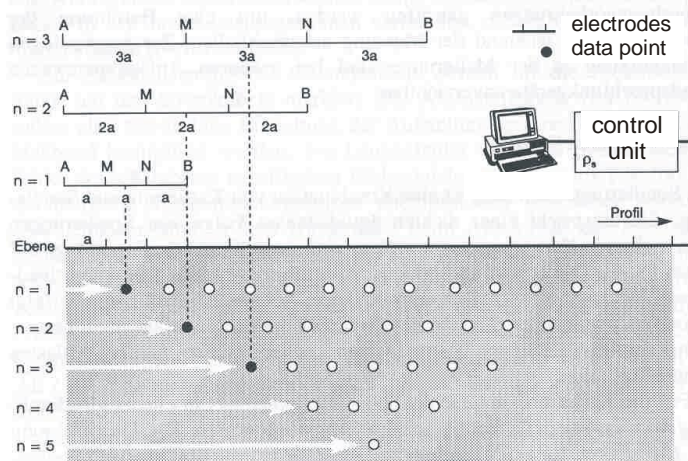
The distribution of ρ_s values depends on the electrodes geometry in respect to the distribution of ρ in the ground (see sensitivity coefficients). This is usually a complex relationship. Even for the simple structure of a vertical boundary between two adjacent homogeneous halves (see example below), the measured ρ_s profiles appear relatively complicated (and of course different for different arrays). For specific cases, measured ρ_s values can even be higher than all existing ρ values in the relevant subsurface (or lower than all existing ρ values) – this is also shown by the examples a and c below.



Theoretical resistivity profiles for different electrode arrays across a vertical boundary (boundary perpendicular to the profile); the resistivities on both sides of the boundary are illustrated by the step like dashed curve.

a. Dipole-Dipole array; b. Pole-Pole array (curve 1) and Wenner array (curve 2); c. Schlumberger array (curve 1) and half-Schlumberger arrays (curves 2,3)

A common concept is the acquisition of pseudosections for 2D-profiling. Pseudosections do not show the true distribution of ρ in the ground (that can be only determined by subsequent modelling) but may already outline the position of structures or objects.



Concept of pseudosection (example of Wenner configuration)

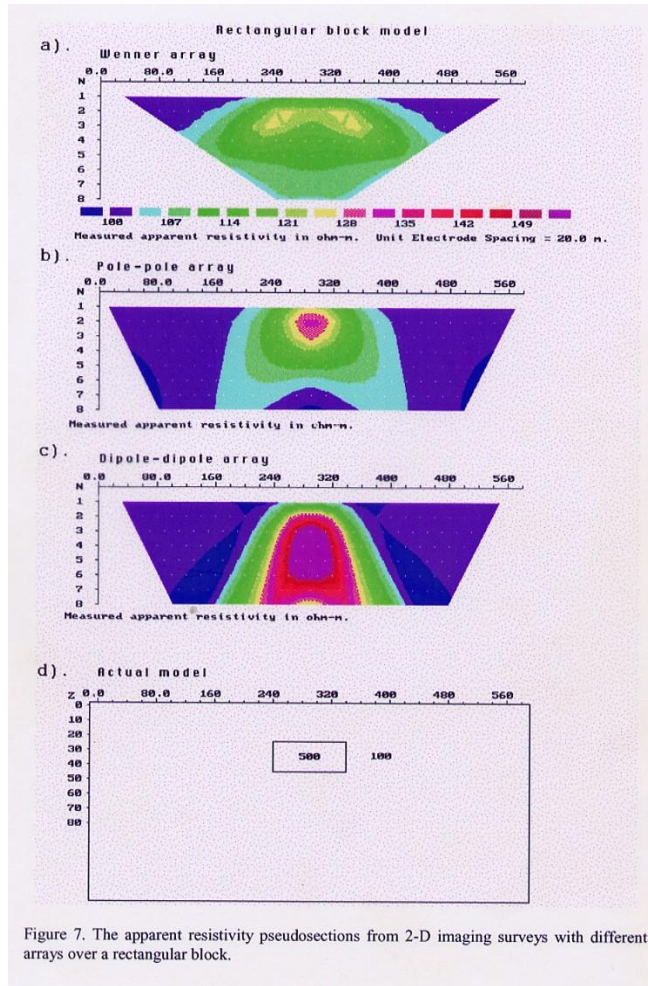
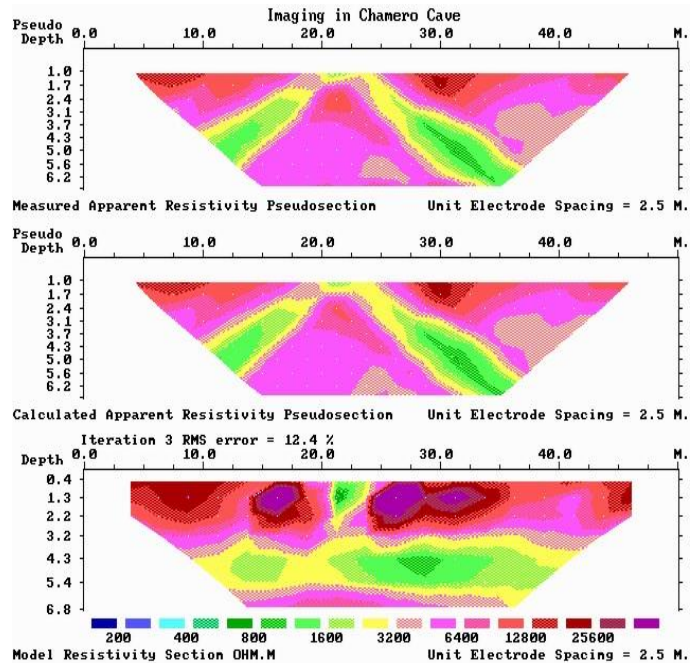


Figure 7. The apparent resistivity pseudosections from 2-D imaging surveys with different arrays over a rectangular block.

Theoretical pseudosections for different electrode arrays over a rectangular 2D-structure

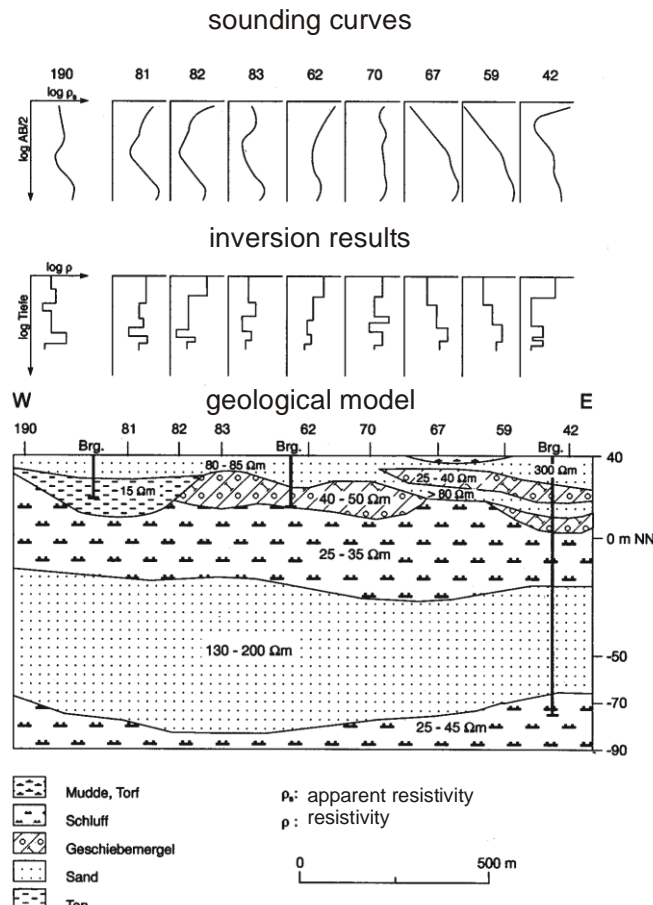


Example: measured pseudosection (top), 2D-model for the resistivity distribution (bottom), and pseudosection calculated from the model (middle).

An alternative approach for 2D-structures:

Combining vertical electrical sounding curves as shown in the example below.

This approach is only possible for not too strong lateral variations. Often this approach gives better results than models from pseudosections (the reason is that for logistic reasons small electrode spacings are underrepresented in pseudosections).

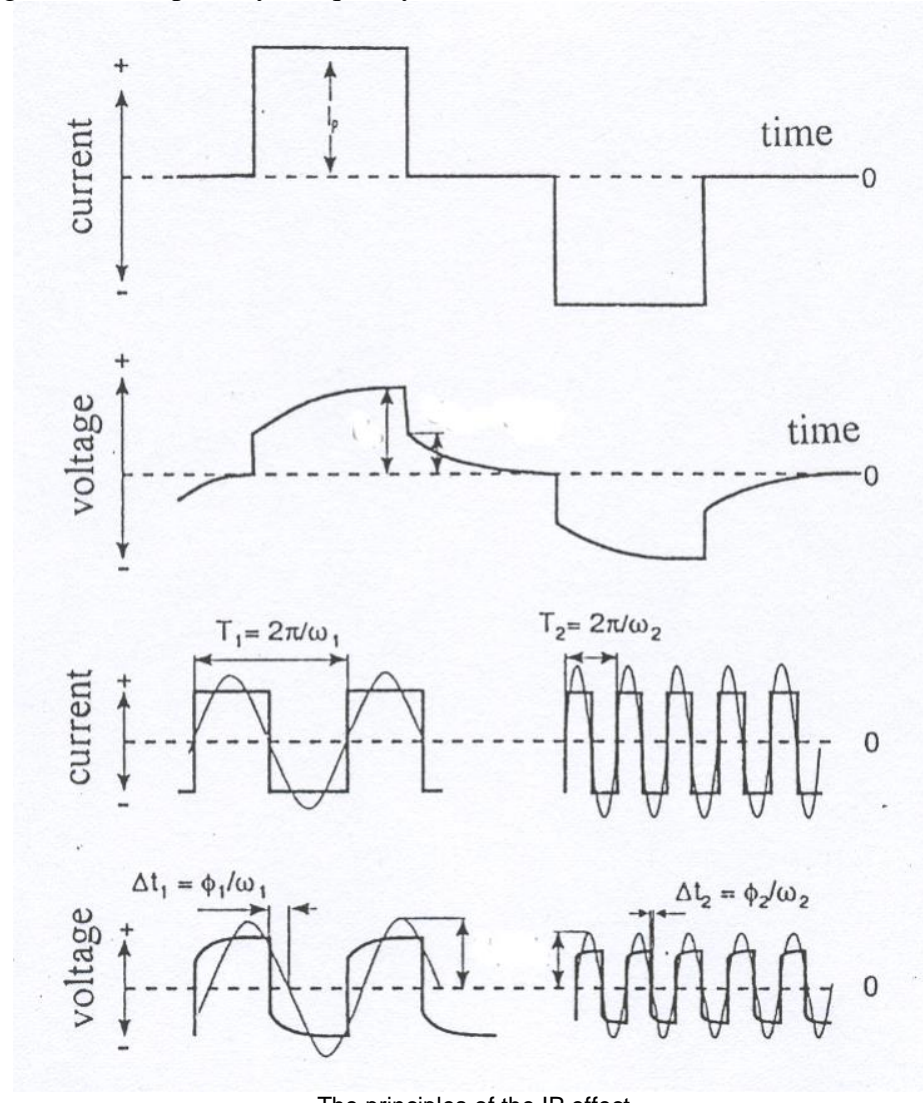


Schlumberger sounding curves, inversion results and the geological model

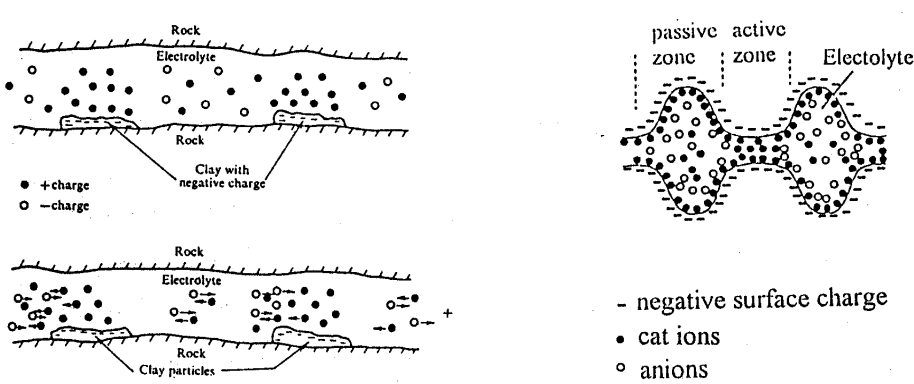
D.4 Induced Polarization (IP)

Measurements of Induced Polarization are performed with the same arrays as DC geoelectrical measurements (VES or profiling). However, the instrument has to be capable to measure the time dependence of the voltage between M and N. A commutating direct current or a low-frequency alternating current is used (in the order of less than 1 Hz to maximum few Hz). The principle of IP is explained in the figure below. It is based on the effect that ground structures can act like a capacitor i.e., when applying a power supply to A,B electrodes certain interfaces are charged up, which takes some time, and when the power supply to A,B is stopped some time is elapsing until these interfaces are discharged again. When the polarity of the current injected by A,B is changing fast, then the time may not be sufficient to fully “charging the ground capacitor” or in other words, the maximum voltage between M,N is not reached. More generally, with increasing frequency of current injection, the maximum voltage is decreasing and the determined ρ_s value is decreasing as well.

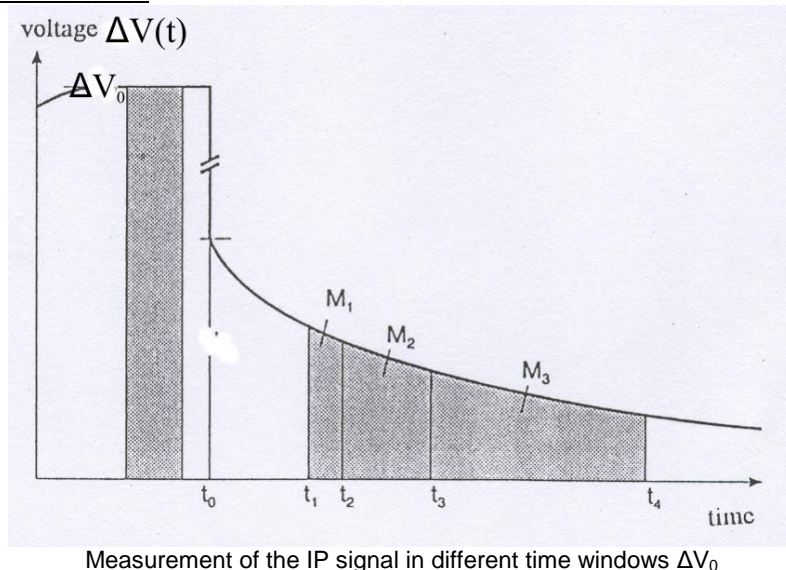
There are two possibilities: (1) one can measure the decay curves of the voltage after shut-off the current (time-domain), or (2) one can compare ρ_s values measured at different frequencies of changing the current polarity (frequency-domain).



Possible causes for IP are chargeable interfaces as occurring for contacts of metal or clay with the surrounding (IP effects are especially strong for contacts with different conduction mechanism):



- a) Ion accumulation at clay mineral surfaces (upper pore channel with normal distribution of ions, lower pore channel with membrane polarization due to an applied voltage). b) Polarization in clay free material.

Time-domain measurementMeasurement of the IP signal in different time windows ΔV_0

$$\text{Chargeability } M = \frac{1}{\Delta t} \cdot \frac{1}{\Delta V_0} \int_{t_1}^{t_2} \Delta V(t) dt$$

(ΔV_0 - voltage reached during current flow, $\Delta V(t)$ voltage decaying with time after current injection stopped; t_1 & t_2 - limits of a selected time interval for measurement, $\Delta t = t_2 - t_1$)
(sometimes the division by Δt is omitted, depending on definition)

Frequency-domain measurement

$$\text{Frequency effect } FE = \frac{\rho_f - \rho_F}{\rho_F} \quad \% \text{ frequency effect } PFE = 100 FE$$

ρ_f, ρ_F : resistivities measured in the frequency ranges of 0.05-0.5 Hz and 1-10Hz, respectively
(resistivities determined by $\rho = K \frac{\Delta V}{I}$)

$$\text{Metal factor } MF = \frac{PFE}{\rho_f}$$

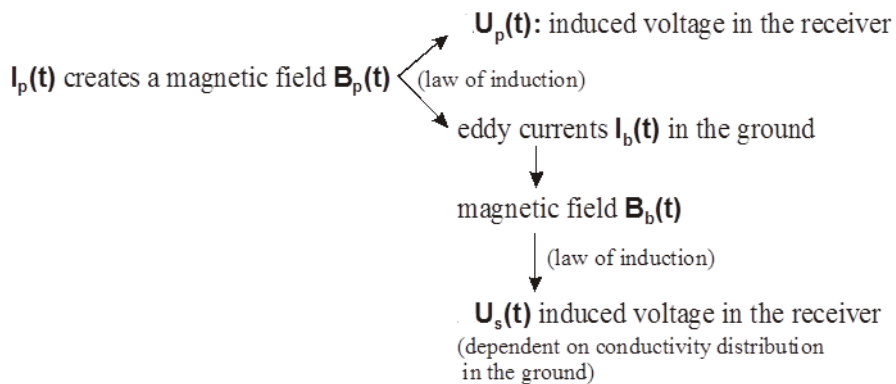
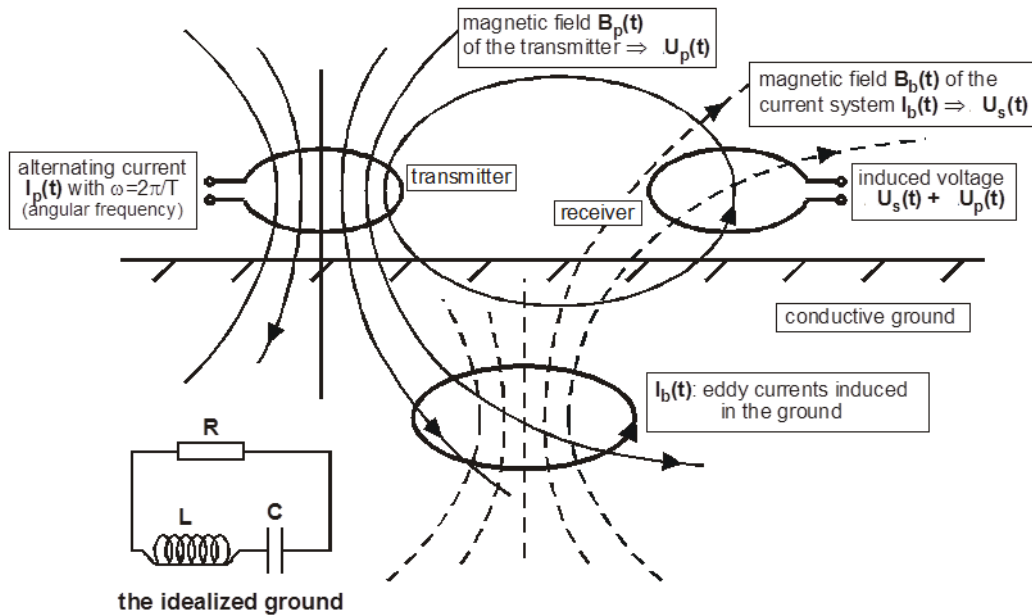
(the use of MF enhances the anomaly across ore deposits, because metals not only show a high PFE anomaly, but at the same time a low resistivity)

D.5 Electromagnetic induction methods

Note: voltage $U = \Delta V$ is used here

D.5.1 Principle of the Slingram method (2-coil method)

An alternating current in a transmitter coil creates an induced voltage/current in the receiver coil and also in the conductive ground, the latter leading to eddy currents. The eddy currents in the ground (alternating currents) also create an induced voltage/current in the receiver coil.



D.5.2 Signal decomposition

measured signal at receiver:

$$U_s(t) + U_p(t)$$

can be eliminated

result: - amplitude of the 0° -phase and 90° -phase of $U_s(t)$

- phase shift of $U_s(t)$ relative to $U_p(t)$

The primary voltage $U_p(t)$ and the secondary voltage $U_s(t)$ are not in phase !

Primary voltage in the receiver coil (created directly by the current in the transmitter coil):

$$U_p(t) = U_{pos} \sin \omega t$$

Secondary voltage in the receiver coil:

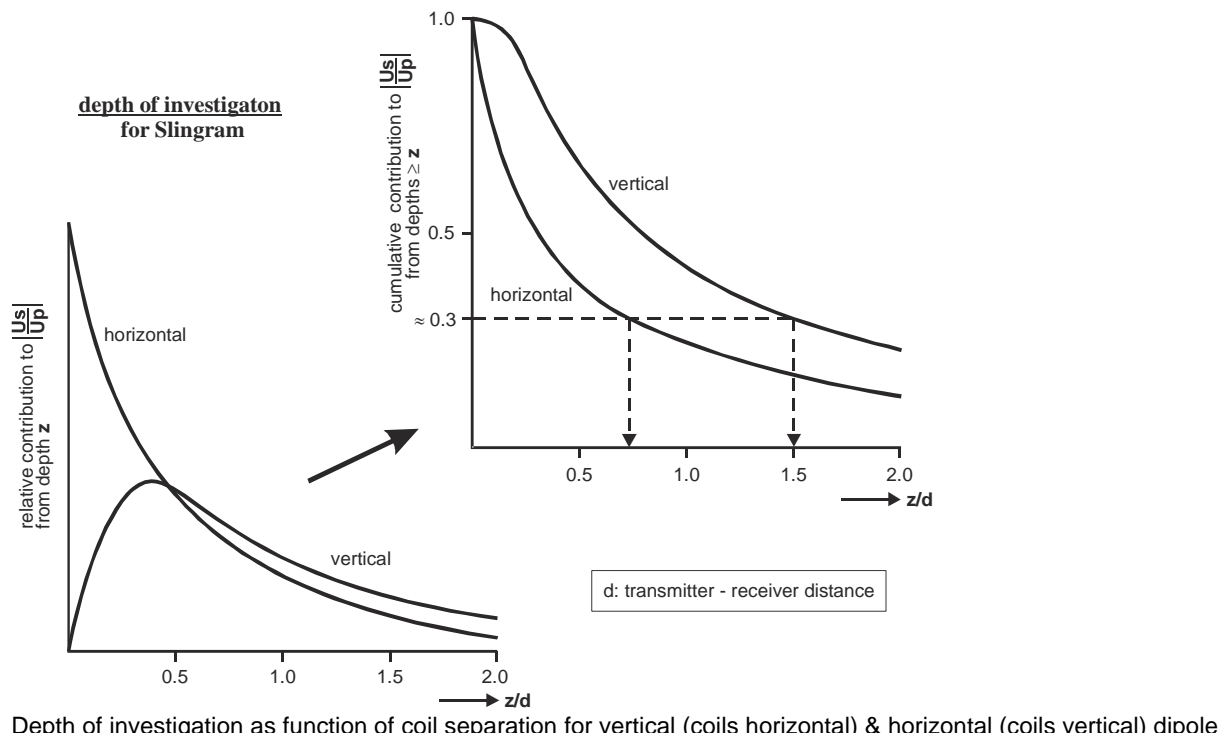
$$U_s(t) = U_{so} \sin(\omega t + \varphi_0) = U_{s_{in}}(t) + U_{s_{out}}(t)$$

In-phase (or also termed 0° -phase, real part Re): $U_{s_{in}}(t) = U_{s_{in}} \sin(\omega t)$

Out-phase signal (90° -phase, quadrature phase, imaginary part Im): $U_{s_{out}}(t) = U_{s_{out}} \cos(\omega t)$

D.5.3 Penetration depth and depth of investigation

A geometrical constraint for the depth of investigation (DOI) is given by the T-R coil separation; it also depends whether the coils are oriented horizontally or vertically.



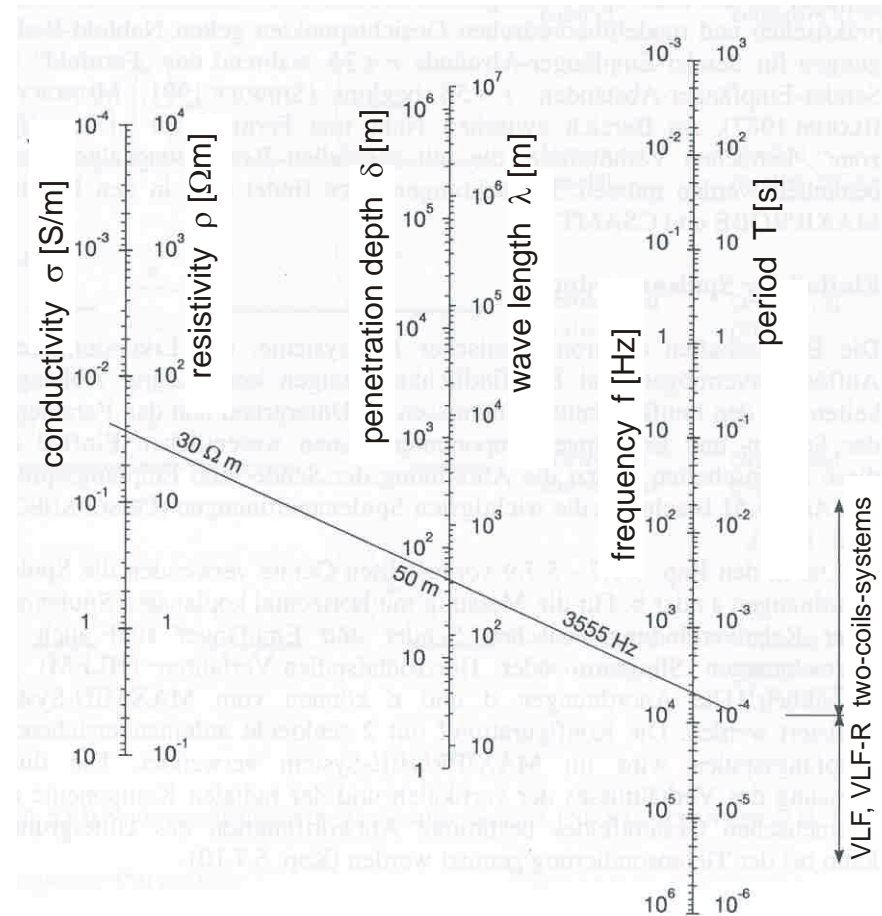
Depth of investigation as function of coil separation for vertical (coils horizontal) & horizontal (coils vertical) dipole

Penetration depth (skin depth δ) $\delta = \sqrt{\frac{1}{\sigma \mu \pi f}}$

(depth, in which the induced signal is decreased to the $1/e$ of its value at surface)

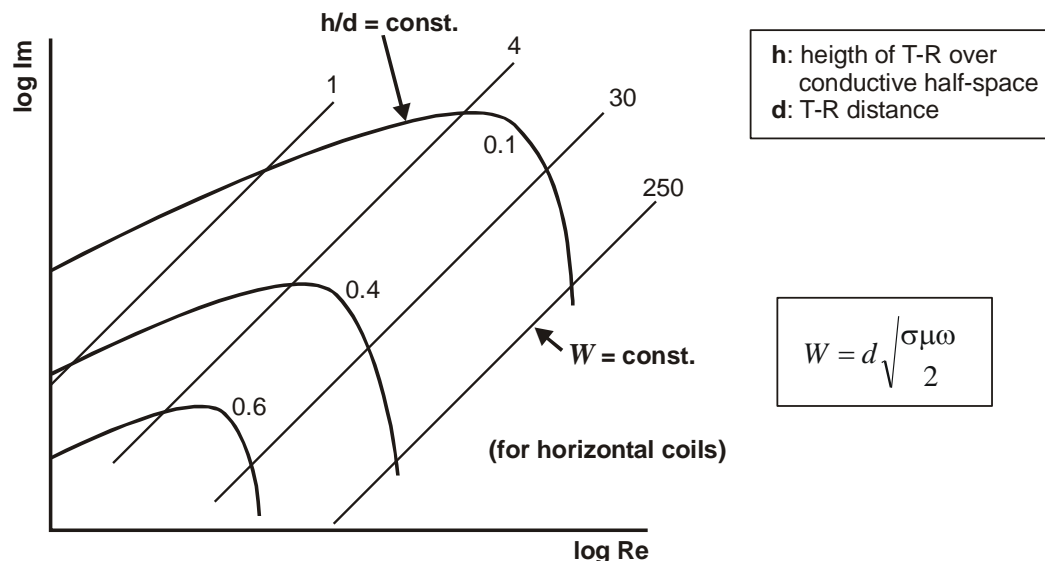
For $\mu = \mu_0$ one gets: $\delta[m] = 503 \sqrt{\frac{\rho[\Omega m]}{f[Hz]}}$ (ρ value in Ωm and the f value in Hz gives the δ value in m)

For sufficiently large coil separation, the Skin depth can become the limiting factor for DOI. For induction methods without a defined T-R distance it is generally determining the DOI (e.g. VLF, magnetotellurics – see further below).



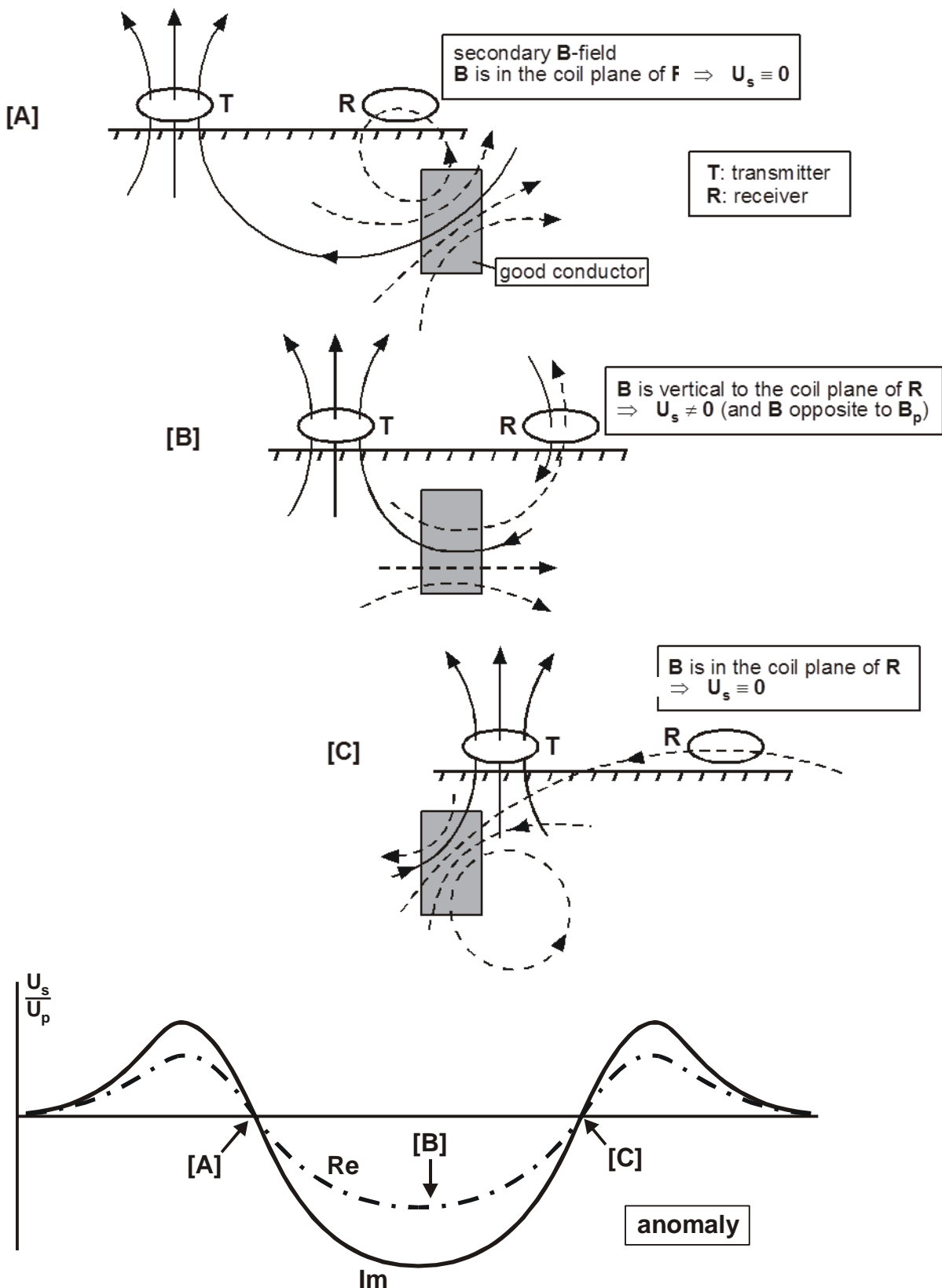
Graphical determination of penetration depth as a function of frequency and resistivity (for half space)

D.5.4 Inversion of Slingram data

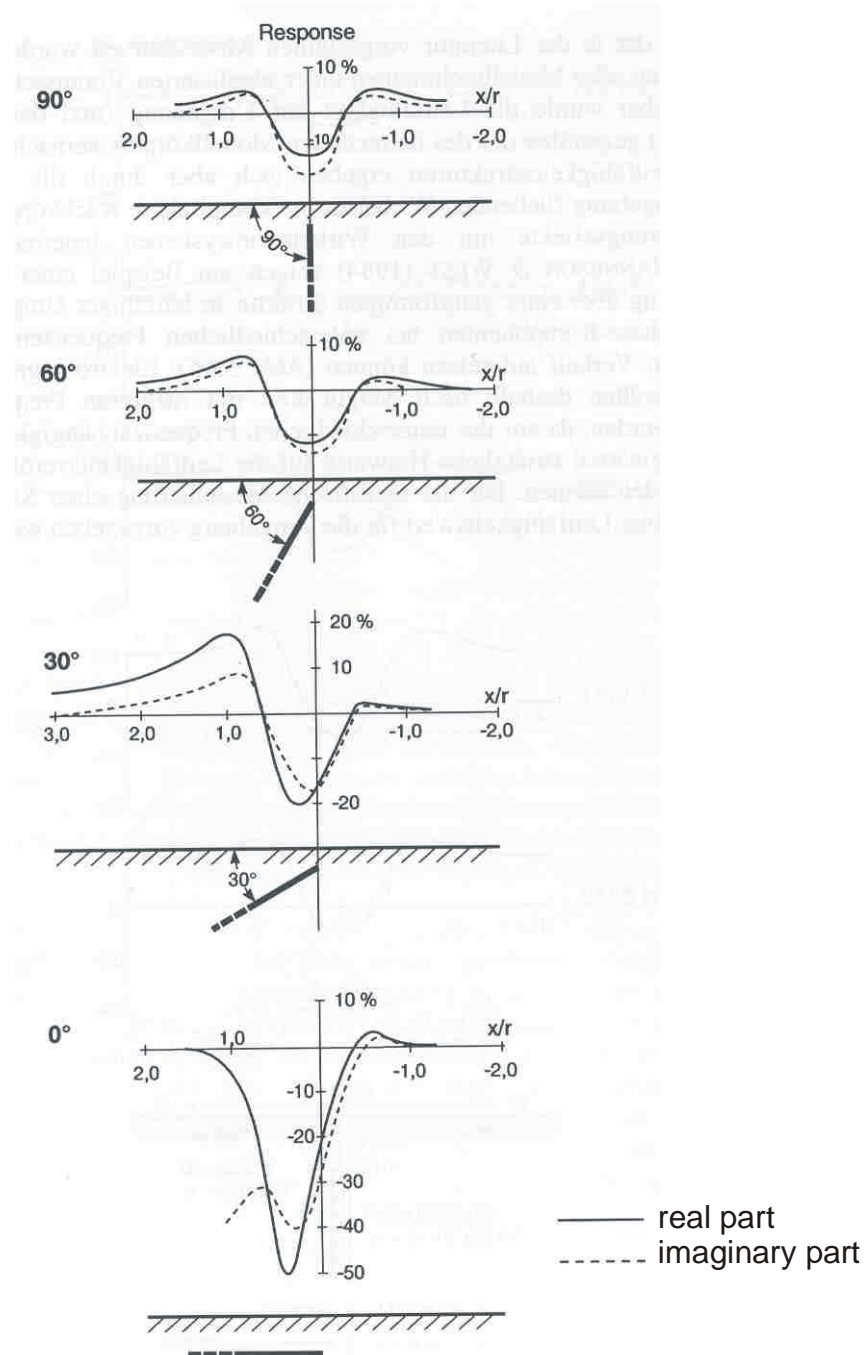


Interpretation of Slingram anomaly (determination of the depth and conductivity of a conductive half space using real (Re) and quadrature (Im) parts of the secondary voltage)

D.5.5 The Slingram anomaly



Sketch for explanation of a Slingram anomaly across a conductive body

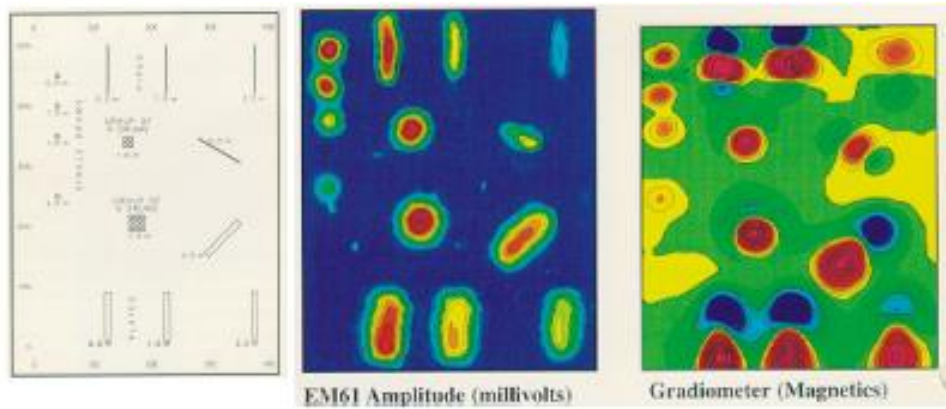


The dip of a conductive plate influences the shape of the Slingram anomaly

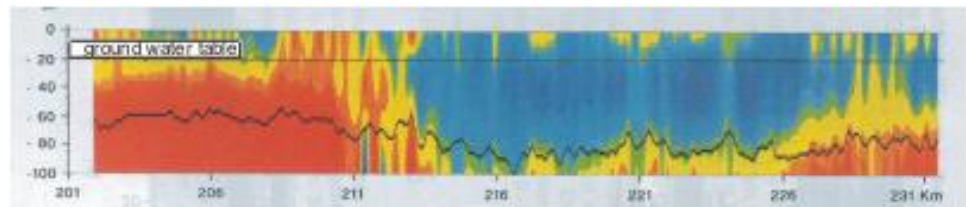
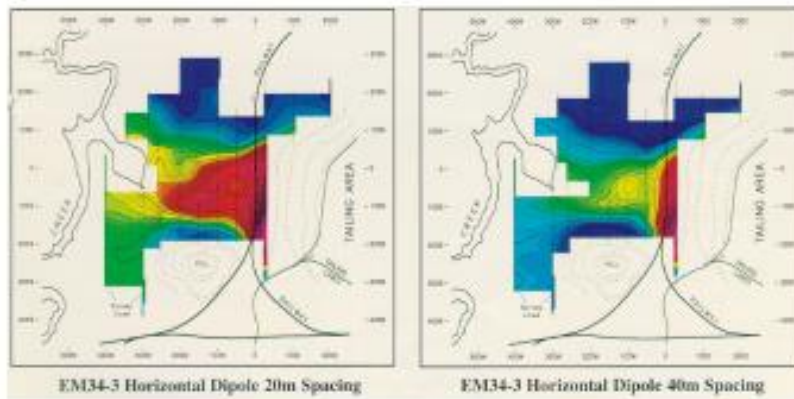
D.5.6 Instruments and examples



Some commercial Slingram instruments (only for the one at the right side, the coil separation and the operation frequency can be varied; the others are only used for mapping)



Comparison of electromagnetic induction anomaly (middle) and magnetic anomaly (right) on a test field with different buried objects



High conductivity (red) due to saline groundwater (aerogeophysical measurement)

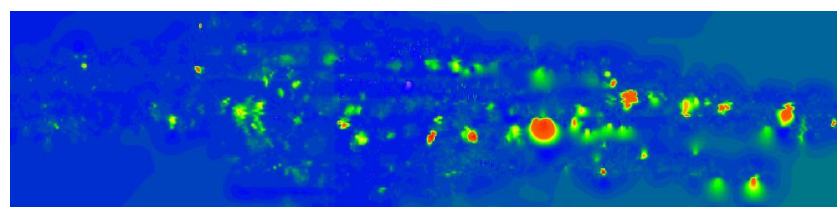
Examples of Slingram anomalies: (top) contamination plume leaking from a former waste disposal site using two different DOI due to coil separation; (bottom) full 2D-inversion of fresh water and salt water distribution

D.5.7 Other induction methods

Transient Electromagnetic Induction (TEM or TDEM)

Principle: The transmitter coil is shut-off and the decaying eddy current field is observed

Advantage: Skin effect is suspended → signal migrates to larger depth (increase of depth of investigation); Disadvantage: Large power required, expensive equipment



TEM example on a military site: metal objects with high conductivity (green & red)

Magnetotellurics (MT)

Principle: Ionosphere currents caused by the sun wind

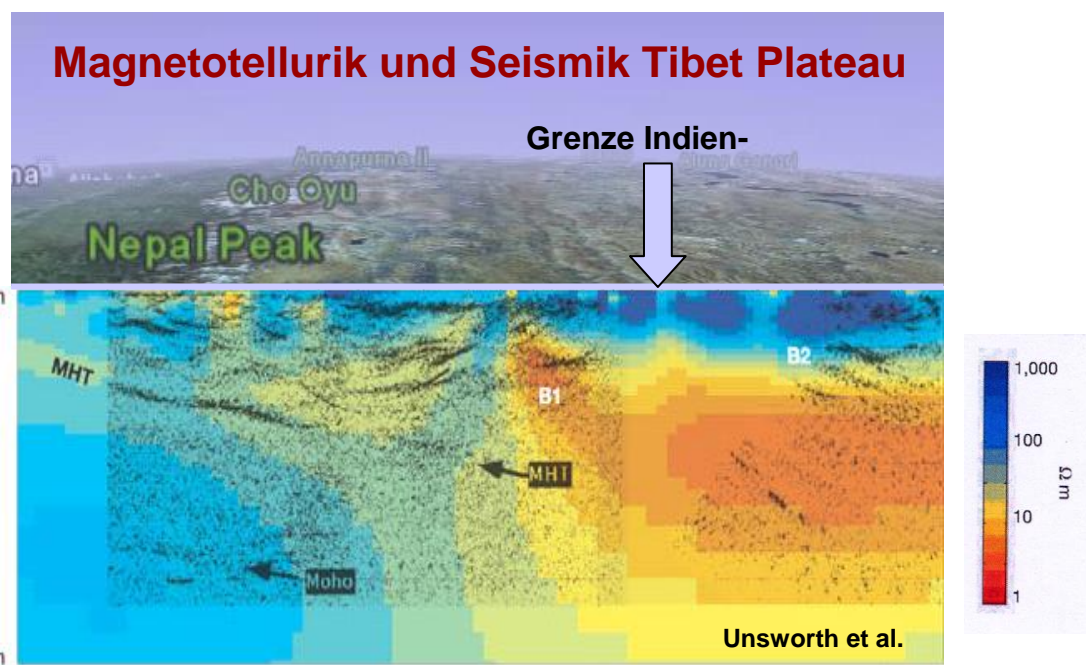
Advantage: High bandwidth of frequencies 0.0001 to 10 Hz → large range of Skin depths
DOI up to few 100 km (Earth's upper mantle)

Disadvantage: Shallow subsurface (uppermost few hundreds m) can be not resolved

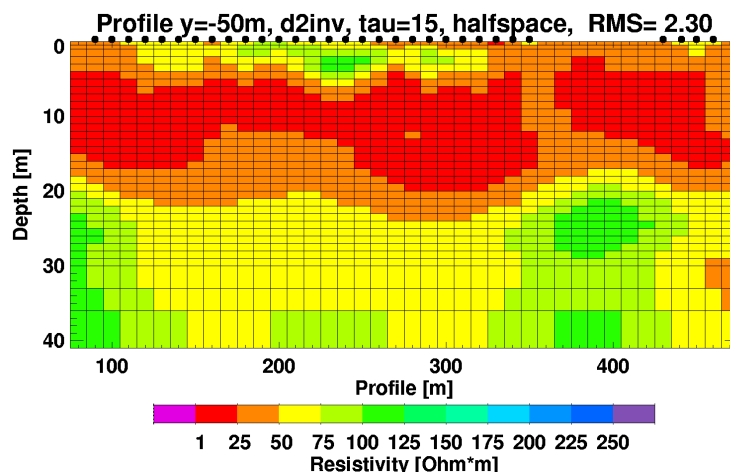
Using higher frequencies of 10 to 10^3 Hz caused by tropical lightning → **Audio-Magnetotellurics (AMT)** (better resolution of shallow subsurface; max. few 100 m penetration depth)

Using even higher frequencies of 10^4 to 10^6 Hz (active radiowave transmitter) → **Radio-Magnetotellurics (RMT)** for very shallow targets (max. few 10 m penetration depth)

A simple version with single low-frequency radiowave signal around 20 kHz is the Very-Low-Frequency (**VLF**) or VLF-resistivity (**VLFR**) method



Magnetotelluric profile across the Himalaya and southern Tibetan Plateau



Radiomagnetotelluric result of a waste disposal site
<http://www.geophysik.uni-koeln.de/forschung/rmt/>

D.6 Electromagnetic wave methods: Ground Penetrating Georadar

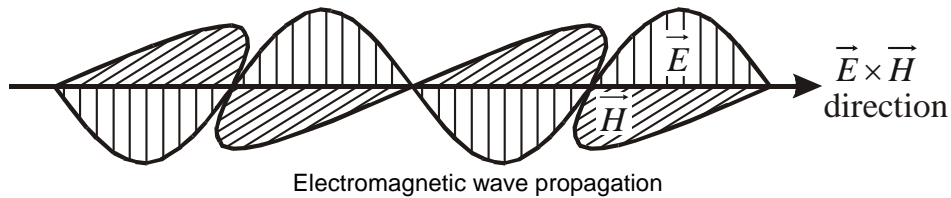
D.6.1 Electromagnetic wave propagation

Starting with Maxwell equations $\text{curl } \vec{H} = \frac{\partial}{\partial t} \vec{D}$ (i.e., no conduction currents) and $\text{curl } \vec{E} = -\frac{\partial \vec{B}}{\partial t}$

one derives the electromagnetic wave equation(s) for plane wave propagation in z-direction in a homogeneous non-conductive space:

$$\frac{\partial^2 E_x}{\partial t^2} = \frac{1}{\epsilon\mu} \frac{\partial^2 E_x}{\partial z^2} \quad \text{and} \quad \frac{\partial^2 B_y}{\partial t^2} = \frac{1}{\epsilon\mu} \frac{\partial^2 B_y}{\partial z^2}$$

(E_x – x-component of E, B_y – y-component of B; $E_y = E_z = 0$, $B_x = B_z = 0$)



The velocity of wave propagation is: $v = \sqrt{\frac{1}{\epsilon\mu}}$.

In free space the velocity is equal to the speed of light: $c = \sqrt{\frac{1}{\epsilon_0\mu_0}} \approx 3 \cdot 10^8 \text{ m/s}$.

Thus in ground: $v = c \cdot \sqrt{\frac{1}{\epsilon_r\mu_r}} \approx c \cdot \sqrt{\frac{1}{\epsilon_r}}$ (μ_r mostly equal to 1 in normal ground material) –

this is useful approximation for velocity in the GPR range (ca. 10 MHz to few GHz)

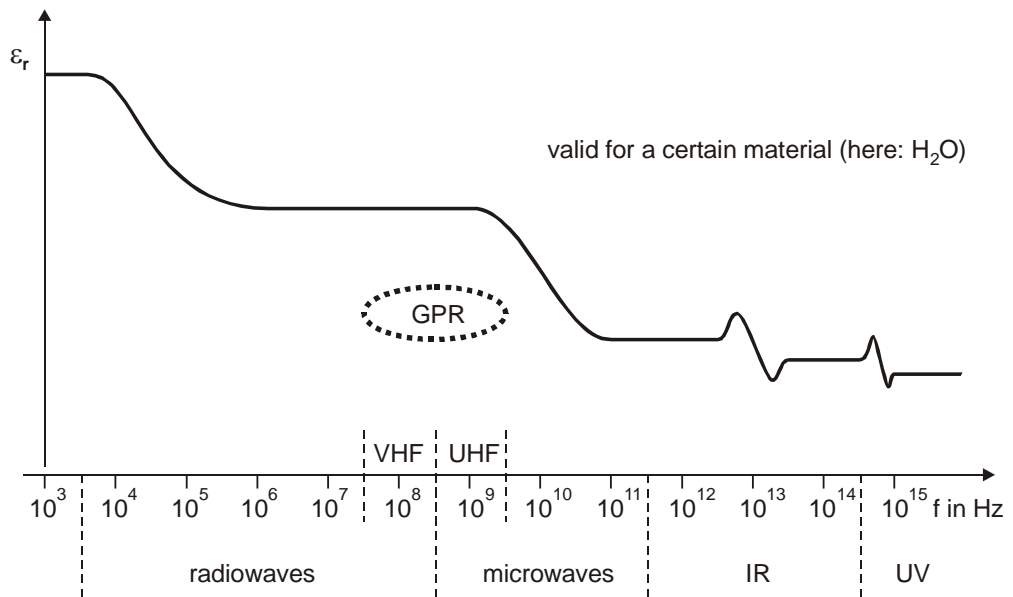
Full solution for plane wave propagation with absorption of energy (conductive space) gives:

$$\text{velocity } v = \frac{1}{\sqrt{\frac{\epsilon\mu}{2} \cdot \left[\sqrt{1 + \left(\frac{\sigma}{\omega\epsilon} \right)^2} + 1 \right]}}$$

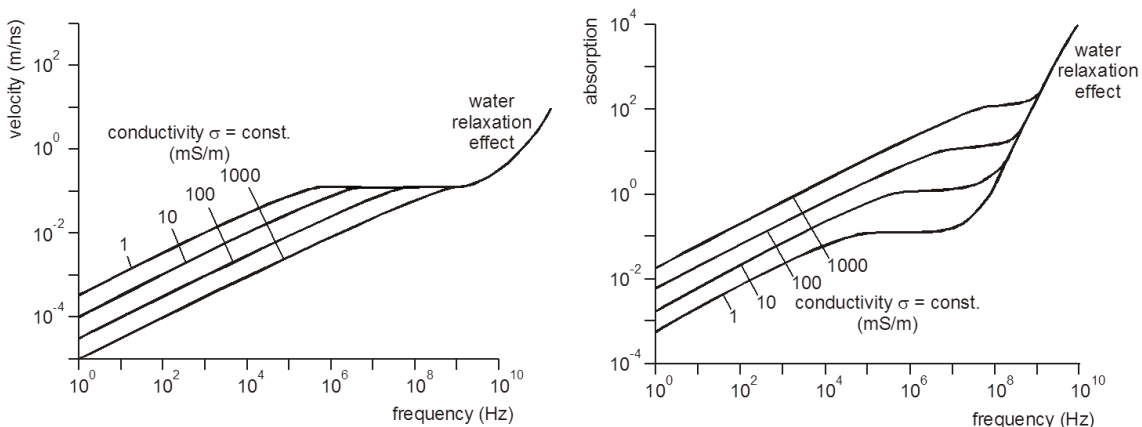
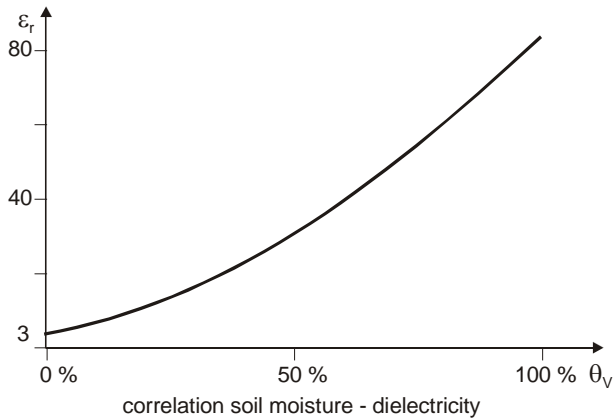
$$\text{absorption coefficient } \beta = \omega \sqrt{\frac{\epsilon\mu}{2} \cdot \left[\sqrt{1 + \left(\frac{\sigma}{\omega\epsilon} \right)^2} - 1 \right]} \quad \text{from } E(z) = E(z=0) \cdot e^{-\beta/z}$$

(σ –electrical conductivity, ϵ – permittivity, μ –magnetic permeability, ω – angular frequency of wave)

D.6.2 Frequency dependence of ϵ , v , β



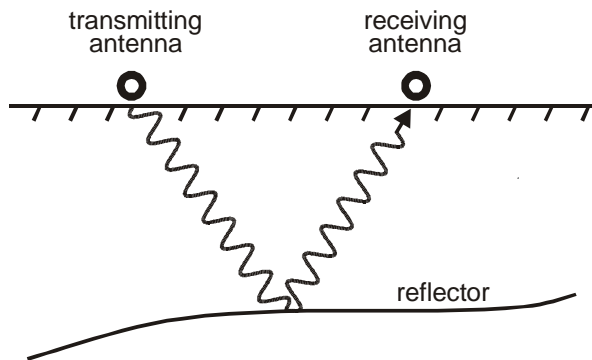
Frequency dependence of the relative permittivity of water □



Frequency dependence of velocity v und absorption coefficient β (in m^{-1}) according to the fundamental formulas above and frequency dependence of ϵ_r

D.6.3 Principles of GPR measurements

GPR measurements are mostly performed in reflection mode



Reflection coefficient (amplitude ratio of reflected wave and incident wave)

$$R = \frac{v_1 - v_2}{v_1 + v_2} = \frac{\sqrt{\epsilon_2} - \sqrt{\epsilon_1}}{\sqrt{\epsilon_1} + \sqrt{\epsilon_2}}$$

ϵ_1 and ϵ_2 are the relative permittivities above and below the reflector.

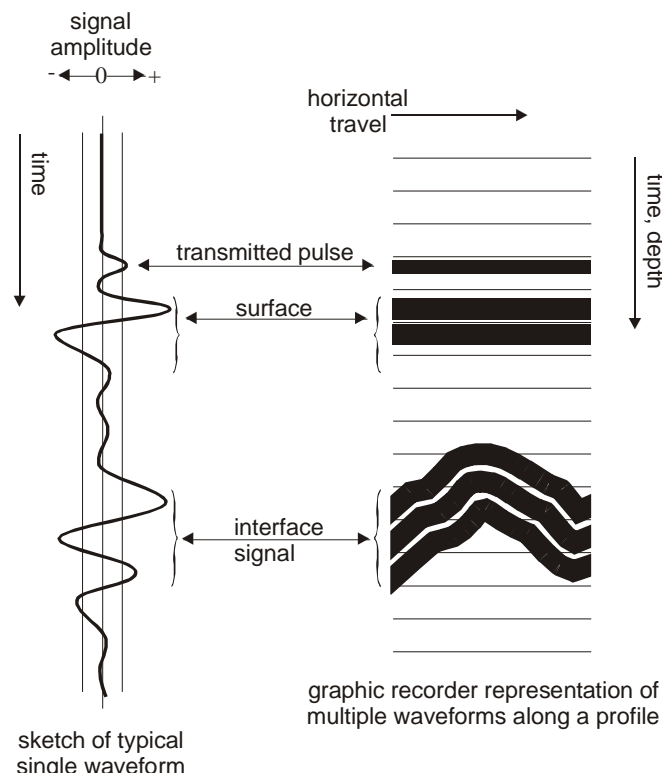
Note: reflectors with high conductivity (e.g. metal objects) do not allow penetration of radar waves, but also create strong reflected signals.

There are two kinds of instrumentation, bistatic (two separate T and R antennas) and monostatic (T and R same antenna, can be switched from transmitting to receiving). Lower frequency instrumentation is mostly bistatic while for higher frequency antenna (above ca. 500 MHz) monostatic equipment is common.

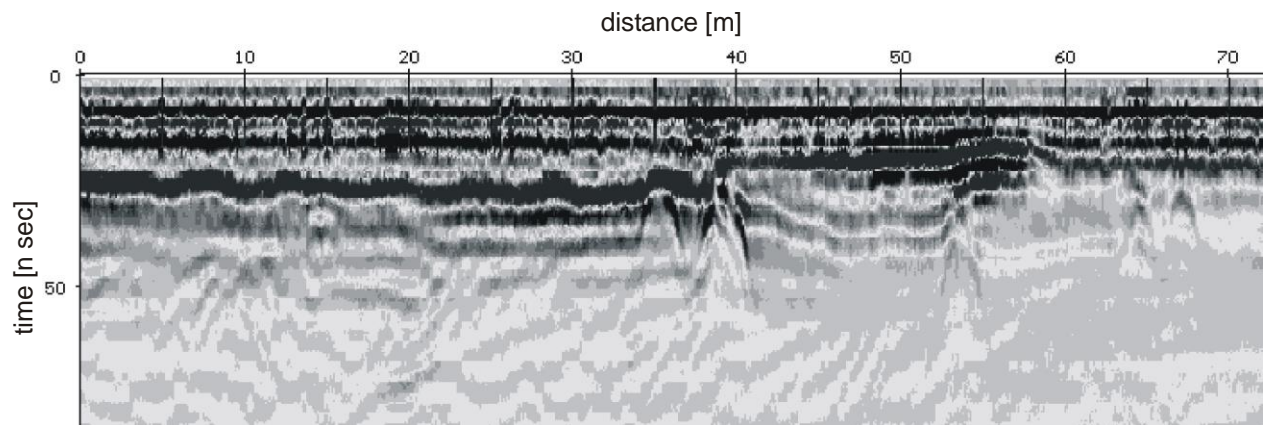
Almost in general, GPR measurements are done with one receiver position, not acquiring CSP data set with subsequent CMP-sorting and stacking (see reflection seismics). With monostatic equipment one is restricted to zero-offset (zero distance between T and R) data acquisition.

The transmitted pulse is usually very short (see figure below). Wave reflection and diffraction can significantly modify the wavelet, making the recorded reflection signal often much longer.

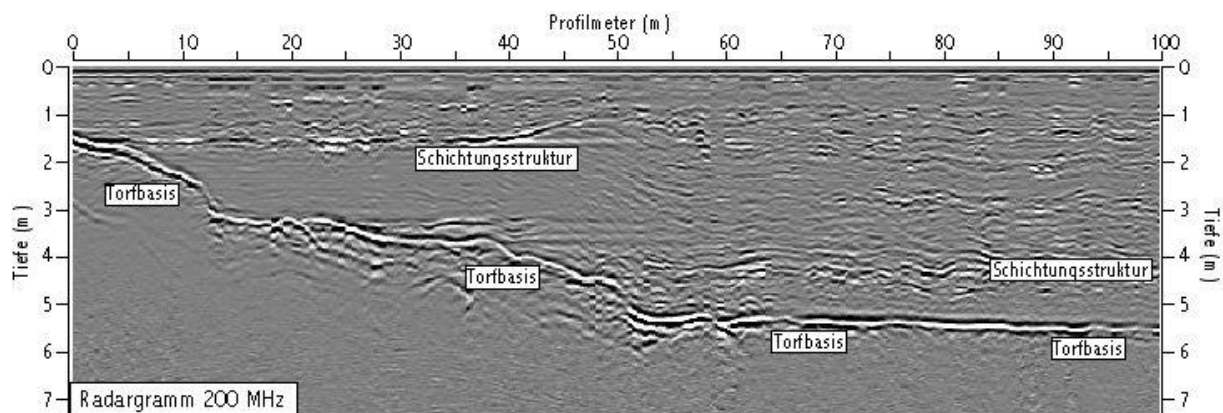
Typically the first signal is a reflection from the surface (monostatic measurement) or a direct wave in air from T to R antenna (bistatic measurement). In both cases the first signal in a radargram appears as meaningless "horizontal stripes" (because the distances antenna-surface or T-R velocity are constant and these waves travel with the speed of light).



Principles of GPR measurements (for the case of monostatic measurement)

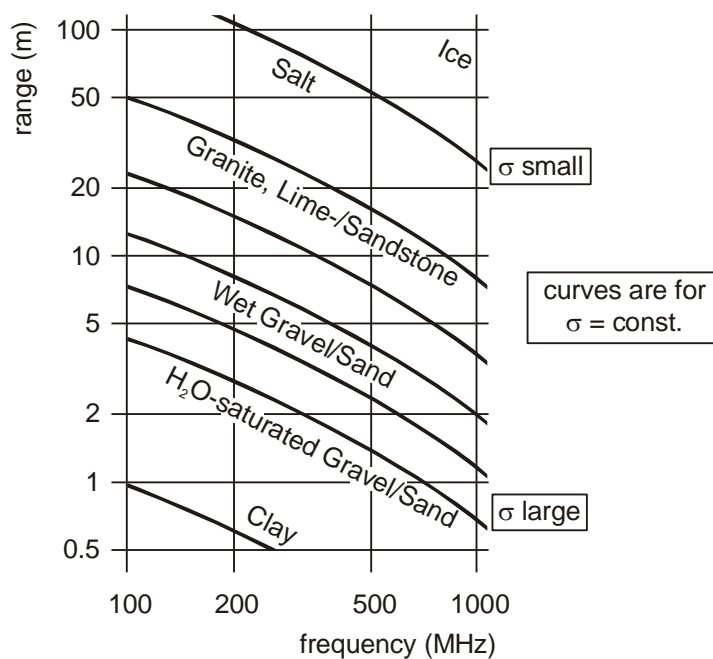


Example for a GPR measurement (showing a very shallow reflector and some hyperbolic structures which are typical in GPR due to smaller objects)



Example of GPR (showing a clear reflection from the base of a peat layer)

D.6.4 Investigation ranges of GPR



Typical investigation ranges of GPR, resulting from damping (absorption) and performance of instruments (ice is by far the best, salt the second-best, in materials with high clay content GPR measurements are impossible)

E Seismics & seismology

See Part II

Geophysical Text Books

(German)

Claußer: Einführung in die Geophysik: Globale physikalische Felder und Prozesse in der Erde, ca. 420 p.

Springer

Bender (Hrsg.): Angewandte Geowissenschaften Bd.II: Methoden der Angewandten Geophysik und mathematische Verfahren in d. Geowissenschaften, ca. 750 p.

Enke

Militzer, Weber: Angewandte Geophysik, 3 Bände, je ca. 350-400 p.

Springer

Knödel, Krümmel, Lange: Geophysik. Bundesanstalt für Geowissenschaften und Rohstoffe (BGR) - Handbuch zur Erkundung des Untergrundes von Deponien und Altlasten, Bd. 3, ca. 1040 p.

Springer

(English)

Telford, Geldart, Sheriff: Applied Geophysics, ca. 750 p.

Cambridge University Press

Sharma: Environmental and Engineering Geophysics, ca. 470 p.

Cambridge University Press

Lowrie: Fundamentals of Geophysics, ca. 340 p.

Cambridge University Press

Robinson, Coruh: Basic Exploration Geophysics, ca. 540 p.

John Wiley & Sons

Griffiths, King: Applied Geophysics for Geologists & Engineers, ca. 220 p.

Pergamon Press